Self-bias On-chip Nanoferrite Circulator for CMOS Integration: Design, Fabrication and Measurement

A thesis submitted by

Tinghao Liang

In partial fulfillment of the requirements for the degree of

Master of Science

in

Electrical Engineering

Tufts University

February 2017

Advisor:

Dr. Mohammed Nurul Afsar

Signature of Author……

Tinghao Liang

Department of Electrical and Computer Engineering

Certified by…….....

Mohammed Nurul Afsar

Professor, Electrical Engineering, Tufts University

Thesis supervisor

Certified by…….....

Valencia Joyner Koomson

Associate Professor, Electrical Engineering, Tufts University

Certified by…….....

Austin Napier

Professor, Physics and Astronomy, Tufts University

Abstract

The overcrowded wireless spectrum and the rapidly increasing need for Giga-bit per second downlink data rate form the driving force of microwave frequency front-end module research and development. The unlicensed 57-63 GHz frequency range is of great importance to the realization of such high speed access point. Modern ferrite microwave devices that are smaller, faster and consume much less power than their active counterparts have been scaled down with help from metamaterials and nanofabrication. Comparing to the traditional, bulky radio frequency ferrite device, their microwave cousins are promising candidates for a critical role in the aforementioned high speed applications.

This thesis presents a complete design, simulation, fabrication and testing of a self-bias, magnetic circulator operating at 60GHz. It features 15dB isolation, 2mm by 2mm size and potential of further integration with CMOS or GaN technology. Simulated and measured results are presented and analyzed together with a detailed fabrication recipe and step by step microscopic photos. This device can be used in applications such as integrated transceiver, phased array radar system, air traffic control and navigation.

Contents

Abstract iii

List of Figures vii

Acknowledgement x

Chapter 1 Introduction 1

1.1 Motivation 1

1.2 Overview of Thesis 3

Chapter 2 Background 5

2.1 Overview of circulator 5

2.2 Different Types of Circulator 9

2.2.1 Junction circulator 11

2.2.2 Differential Phase Shift Circulator 12

2.2.3 Faraday rotation circulator 13

2.3 Overview of Ferrite Magnetic Material 15

2.3.1 Cubic ferrite 16

2.3.2 Spinel ferrite 16

2.3.3 Garnet ferrite 17

2.3.4 Hexagonal ferrite 18

2.3 Overview of nanofabrication 19

2.3.1 Photolithography 19

2.3.2 Deposition Techniques 21

2.3.3 Etching 23

2.4 Review of Barium Hexagonal Ferrite Film Deposition Techniques 24

2.5 60GHz Unlicensed Frequency Band 25

Chapter 3 Characterization of hexagonal ferrite 28

3.1 Free-space quasi-optic spectroscopy system 28

3.2 Characterization of hexagonal nano-ferrite and composite 32

3.3 Study of thermal annealing on ferrite film on GaN-on-SiC substrate 36

Chapter 4 Design, simulation and fabrication of ferrite circulator 41

4.1 Overview of transceiver front end module 41

4.2 Design and simulation of circulator 43

4.3 Detail Fabrication of Circulator 47

4.3.1 Recipe One with lift-off patterning 48

4.3.2 Recipe Two with Chemical-Mechanical Planarization (CMP) 55

Chapter 5 Results and Analysis 59

5.1 Measurement setting 59

5.2 Results of Circulator on Wafer 62

Chapter 6 Conclusion 65

6.1 Future Work 65

6.2 Summary 66

Bibliography 68

List of Figures

Figure 2.1: 3 ports and 4 ports circulator and the direction of energy flows inside of them [7] 5

Figure 2.2: Circuit symbols for a. 3 ports circulator and b. 4 ports circulator [7] 6

Figure 2.3: Circulator functioning as duplexer in a transceiver system 7

Figure 2.4: Different categories of circulator 10

Figure 2.5: 3D model of stripline circulator [6] 11

Figure 2.6: Standing wave inside operating circulator [7] 12

Figure 2.7 Structure of phase shift circulator [7] 13

Figure 2.8 Schematic diagram of Faraday rotation in a ferrite magnetized medium [9] 14

Figure 2.9 Schematic diagram of a Faraday rotation circulator [7] 15

Figure 2.10 (a) Spinel unit cell structure (b) octahedral site and (c) tetrahedral site 17

Figure 2.11 Unit cell of Barium hexagonal ferrite $BaFe_{12}O_{19}$ [10] 18

Figure 2.11 Processes of photolithography and pattern transferring 20

Figure 2.13 Atmospheric attenuation spectrum of free space propagation [26] 26

Figure 3.1 Schematic of setup of free space quasi-optic spectrometer with Backward Wave Oscillator (BWO) source 29

Figure 3.2 Picture of free-space quasi-optic spectrometer in millimeter wave frequency 30

Figure 3.2 Transmittance of hexagonal Barium (Left) and Strontium (right) nanopowder 32

Figure 3.3 Transmittance of hexagonal Barium nanoferrite composite (left) and hexagonal Strontium nanoferrite composite 34

Figure 3.3 Real (Top) and Imaginary (Bottom) part of Permeability of hexagonal Barium ferrite composite and pure Barium ferrite nanopowder 35

Figure 3.4 Photos of Muffle furnace employed for high temperature heat processing 37

Figure 3.4 Transmittance of pure barium ferrite powder, ferrite composite before and after heat treatment at 600°C..... 38

Figure 3.5 Real (Top) and imaginary (bottom) part of permeability of pure powder, ... 39

Figure 3.6 Complex permeability and refractive index of GaN-on-SiC over air reference in Q band 40

Figure 4.1 Schematic diagram of amplitude modulation front end with circulator as duplexer ... 42

Figure 4.2 Three dimensional model of circulator design..... 44

Figure 4.3 Circulator model in real aspect ratio in CST microwave studio 46

Figure 4.4 Gyrotropic model of ferrite permeability as simulated in CST microwave studio 46

Figure 4.5 S-parameter results of 3-port circulator from 45GHz to 80GHz 47

Figure 4.6 Process flow of double liftoff patterning 49

Figure 4.7 Process of ground metallization and dielectric deposition (#1), first lithography (#2), dielectric etching (#3), via plate filling (#4), Second lithography (#5) and center disk etching (#6) 51

Figure 4.8 Microscopic photos of fabricated ground vias for probe landing 52

Figure 4.9 Process of 3rd lithography (#7), aluminum sacrificial layer deposition (#8), 1st liftoff (#9), ferrite composite deposition (#10), 2nd liftoff (#11) and transmission line deposition (#12) 53

Figure 4.10 Microscopic photo of circulator after center disk was etched (top left), after aluminum deposition (top right), after double-liftoff was finished (bottom left) and after transmission line metallization (bottom right) 54

Figure 4.11 Mylar mask design for first (left), second (middle) and third (right) lithography 55

Figure 4.12 Process of Electroplated ground via fillings (#1), ferrite composite spin-casting (#2), Chemical-Mechanical Planarization (#3) and transmission lien metallization (#4) 57

Figure 4.13 Microscopic photo of device after Chemical-Mechanical Planarization 58

Figure 4.14 Microscopic photo of fabricated circulator on wafer 58

Figure 5.1 Probe from CascadeMicrotech and N5227A network analyzer from Keysight 60

Figure 5.2 Photo of circulator on-wafer probing setting during measurement 61

Figure 5.3 Microscopic view of fabricated circulator under test 61

Figure 5.4 Measured S-parameter of circulator 62

Figure 5.5 Scanning Microscopy Image of ferrite composite surface 63

Acknowledgement

I would like to thank the individual and organization that made this research and thesis possible. First and for most, I would like to express my gratitude to my research advisor: Professor Mohammed Nurul Afsar. He accepted me as a member of his research group and brought me all chances and opportunities that I could never have imagine. He not only provided me with technical assistance but also caring in life. His respect to my decision on not continuing toward PhD degree is very heart warming. He is a truly supportive advisor who gave me full trust and encouragement I need.

A special thanks is warranted for Professor Valencia Joyner Koomson. Her devotion and contribution to this project is the most crucial thrust to this project. She provided me with all support I needed including facilities and equipment access at Harvard University and MIT. Her professional network and long experience played an essential role in leading the project toward right direction. Her valuable comment and advice guided me in each and every step.

I would like to thank Professor Robert White for his help and guidance throughout the fabrication process. His knowledge in fabrication is of great value to this project for every single tip from him could save us both energy and time. He guided me through metal plating process and generously shared his recipe of plating with me.

I also want to thank Professor Austin Napier for his lectures on electromagnetic theory. His teaching is full of wisdom and his thorough derivation inspired me. In my final presentation in class his questions about circulator project enlightened me to think about problems in more insightful way in my later research and study.

Meanwhile, I should thank Dr. James K. Vlahakis for his well-structured training, well-organized documents and well maintenance in cleanroom. His is always the first person I turned to when I met problems in lab and need help for trouble shooting and mostly importantly he was always ready and willing offer help.

Additionally, I would like to thank Liu Chao for his help and contribution to this project together with advice and encouragement throughout my graduate study. His spectrum of knowledge was incredibly wide and he was the person who knew the most about the project. Besides the role of a colleague, he is also a friend and a model that I'm always learning from.

Moreover, special thanks to Jun Jadormio, his in-depth knowledge of RF and microwave circuit is a great asset to any research group or company. Warm-hearted as he is, he gave me a great deal of advice and assistance in academic life and future career building. He also kindly allowed me to borrow testing equipment from Qorvo and helped me to calibrate and probe circulator on wafer. This project could not make this far without him.

I would like to thank Miriam L. Santi, for her big help in dealing with order of supply and reimbursement for traveling. She was always patient dealing with all my questions and requests. I appreciate all efforts she made to assist this project.

Finally, I want to thank my parents Nianchun Li and Feng Liang, for everything they have done for me throughout my life. They believed and encouraged me to move forward to higher education and provided me with whatever they could give. Their unconditional love and continuing support are the roots of any trivial success I have achieved in my life.

Last but not least, I want to thank Junrui Cheng, my significant one. She hold my hand on the verge of my falling and lighted my beacon at the crossroad of this life journey.

Chapter 1 Introduction

1.1 Motivation

The work of this thesis originates from the need of an on-chip circulator that would replace traditional bulky circulators with a miniature, self-bias planar device featuring potential of integration with existing CMOS or GaN-on-SiC technology. The driving forces of intensive research in this field are the rapidly increasing needs of a high speed wireless communication system that asks for Giga bits per second and even higher data rate and the booming wireless device market.

If we decompose a modern wireless communication system, the functions of all major components fall into two categories: processing and transmitting/receiving. The transmitting/receiving modules, or in their other name “transceivers”, are the interface of a wireless communication device with outside. A circulator can play an important role in “merging” the two paths of transmitting and receiving and provide other advantageous features.

More specifically, the circulator is a three ports (or in some rare cases four ports) passive and non-reciprocal device that guides microwave and radio frequency signals that are fed into it to flow in a circulating manner and exit from specific ports. By proper design, it can be made that one port becomes “invisible”, or in a microwave engineer’s word, isolated from another port. However

reversely the port can see a through path to that port without problem. This is the non-reciprocal property of the circulator. Circulators have been widely used in microwave systems as duplexer, isolator, multiplexer and in applications such as parametric amplifier etc. [1]

The non-reciprocal performance of the circulator derives from ferrite material that can provide anisotropic field. Traditionally, circulators are bulky and cumbersome because the ferrite material in use requires biasing field from an external permanent magnet. It increases not only the weight and size, but also the cost of a complete device. Aforementioned circulators are mostly used as a stand-alone device that shows no evidence of ability to integrate with an IC. Another factor that limit previous attempts from shrinking the size of circulator is, in order to first sustain then guide microwave energy, the center part of the circulator is substantially a microwave resonator, whose size is inversely proportional to signal frequency or in another word, proportional to wavelength. For instance a circulator works in 1 GHz frequency range can be as large as 6cm* 6cm* 3cm [2]. Common wireless communication applications like cell-phone and WIFI operate in a frequency range lower than 6 GHz, in which the circulator has no competiveness against other duplexing solutions like T/R switch and BAW/SAW filtering.

However as the need for higher data rate wireless solutions increasing, next generation (5G) communication will be likely to operate at much higher frequency [3]. The decision of Federal Communications Commission (FCC) to allocate 57-64 GHz band for unlicensed use has sparked intensive interest to develop wireless communication systems operating in these frequencies. This unlicensed band featuring high air absorption in free space propagation, which enables frequency re-use and most importantly several Giga bits per second data rate for end users. Such 5G trials have been deployed in the Tokyo metropolitan area recently to test targeting speed of 10 Gbps [4]. Meanwhile, at 60 GHz frequency range, the size of resonator within circulator falls into sub-millimeter range and firstly become dimensionally comparable to other millimeter wave integrated circuit features size [5]. Regarding biasing magnet that was impeding miniaturization of circulator,

here in Prof. Afsar's group, the Millimeter and Sub-millimeter Wave Lab, we have extensive preliminary results of ferrite characterization and measurement. Out of all types of ferrite material we examined, Barium hexagonal ferrite shows unique features of low loss, high permeability and most importantly, strong anisotropic field that can sustain itself after the external biasing magnet is removed. These features derive from its special hexagonal crystallization and these preliminary results help us to remove the last obstacle in the way. With all these fact in combined, an on-chip self-bias circulator operating at 60 GHz is now promising and feasible.

In collaboration with Dr. Koomson's group with extensive experience in CMOS IC design, we develop a cost-effective and time-efficient way to fabricate and pattern Barium ferrite material on silicon wafer. The outcome of this thesis is the design, simulation, fabrication and testing of a very low cost on-chip circulator employing this method. Such circulators featuring self-bias and 2mm by 2mm size, we believe is the smallest circulator that has ever been made so far. This is a very fast fabrication recipe that can be implemented in 2-3 days and hundreds of circulators can be produced on one four inch silicon wafer. We also investigate the possibility of migrating this recipe from silicon wafer to GaN-on-SiC wafer to enable high temperature processing that can greatly improve ferrite performance.

In conclusion, works presented in this thesis attempt to address the huge need for a miniature circulator with reasonable cost. We'd like to explore the feasibility of on-chip circulator as duplexer used in integrated transceiver as a solution to next generation wireless communication.

1.2 Overview of Thesis

This thesis is divided into five chapters. Firstly, in background chapter, the fundamental knowledge will be introduced to lay the solid ground for understanding. Variety of topics will be covered. Section 2.1 provides a brief overview of circulators and section 2.2 will cover the topics

of different types of the circulator out there and the characteristics of each and every type. In the next section is the introduction of the most critical building block: ferrite material. Different types of crystallographic structure of ferrite material will be introduced and we will take a closer look at the special hexagonal ferrite that enables the non-reciprocal performance of circulator. Following this section, we have an informative section about state-of-art nano-fabrication techniques and tools that were utilized in this work. Chapter 2 ends with short review of common ferrite deposition method and characteristics of 60 GHz unlicensed frequency band.

In Chapter 3, characterization methodology of nano-ferrite material in microwave frequency range will be introduced and experimental results acquired by employing a free-space quasi-optic spectrometer will be analyzed and discussed. The investigation of high temperature annealing influence on ferrite properties will also be presented in this chapter.

In Chapter 4, detailed explanation of principle of circulator will be presented on the basis of preliminary background knowledge. Design methodology and derivation will be provided with example discussed in the first section. Section 3.2 will cover simulation setup and full-wave EM simulation results of our design. In the next section, preparation and deposition technique of ferrite thin film will be discussed. Characterization results of our ferrite thin film employing measurement techniques introduced in previous chapter will be presented in this section. Section 3.3 goes over the complete recipe of device fabrication and pros and cons of two different paths toward final device.

In Chapter 5 we lay down the results of the circulator measured on network analyzer at operating frequency. Final results will be analyzed both quantitatively and qualitatively for future improvement. We will present the proposed solution to problem we found after measurement.

The last chapter is a summary of the works performed and the future outlook.

Chapter 2 Background

2.1 Overview of circulator

The circulator is a passive, non-reciprocal ferromagnetic device that has either three or four ports, where power can be transferred from port to port in a circulating sequence. [6] Its non-reciprocal property enables us to control RF or microwave power to flow in a specific direction, hence making it useful as a building block of RF/Microwave system.

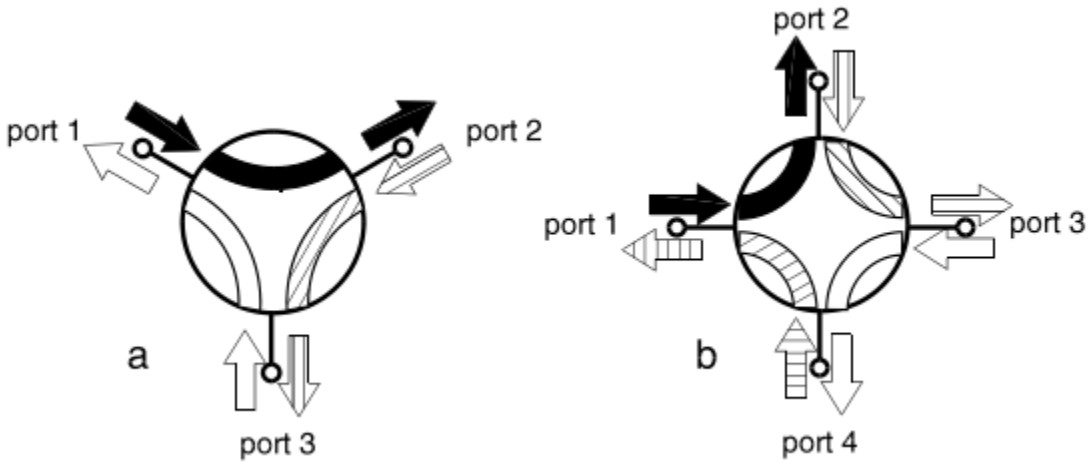

Figure 2.1: 3 ports and 4 ports circulator and the direction of energy flows inside of them [7]

A figure of 3 ports and 4 ports circulator is shown in Figure 2.1. As in the most common three ports case, power fed into port 1 would only flow to and exit at port 2, while port 3 is “invisible” or in more technical word, decoupled. At the same time, power going in from port 2 will only go directly to port 3, ignoring port 1. Similarly if we feed power in from port 3, it can be only received at port 1 but not port 2. In a four ports circulator power flows in similar circulating manner: signal that is fed into one port can only be present at the port right next to it, in either clockwise or counterclockwise manner. If there is reflection at the output port with highest priority, for example if port 2 is open rather than matched load, then signal coming from port 1 will bounce back and go to port 3 like it was fed in from port 2.

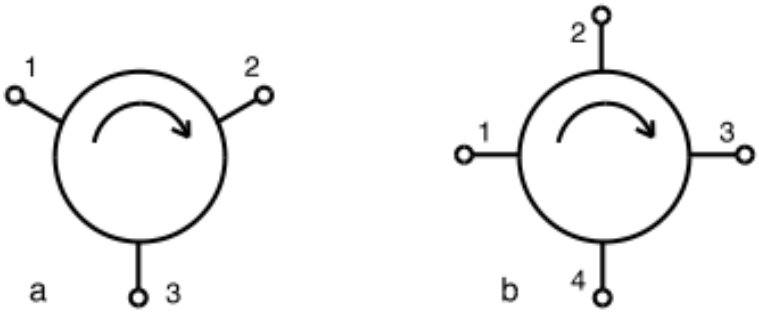

Figure 2.2: Circuit symbols for a. 3 ports circulator and b. 4 ports circulator [7]

The circuit symbols for 3 ports and 4 ports circulator can be found in Figure 2.2, in which the arrows represents the direction of power flow, either clockwise or counterclockwise. This can be explained more explicitly in the language of scattering matrix. The scatter matrix of an ideal circulator with all three ports matched to characteristic impedance should be as follows:

$$[S] = \begin{bmatrix} 0 & 0 & 1 \\ 1 & 0 & 0 \\ 0 & 1 & 0 \end{bmatrix}$$

This means the power is transferred from port 1 to port 2, from port 2 to port 3 and in a circulating manner, from port 3 to port 1. This intrinsic direction cannot be reversed unless the polarity of biasing field inside the circulator is flipped.

If we terminated one port with matched load then the circulator is easily turned into an isolator. An isolator is another non-reciprocal passive microwave device in which power can only flow unilaterally. It is widely used in scenarios when a sensitive block of the system needs to be separated from outside or inside reflected power, or to protect the component from excessive power saturation. One of the application examples is to use the circulator as an isolator in noise figure measurement with Faraday box and Noise Figure Analyzer (NFA). Noise generated from a noise source is fed from outside of Faraday box to Device under Test (DUT) inside of box. However if any noise reversely goes through the input cable and is reflected back, this component of power will be added on internal noise figure and measurement error will be introduced. If we insert an isolator at the interface of input cable and DUT, this reflected signal will be attenuated when it comes back and becomes negligible. The power level loss across isolator can be compensated by hooking up a high gain pre-amp after DUT, which can de-embedded during calibration.

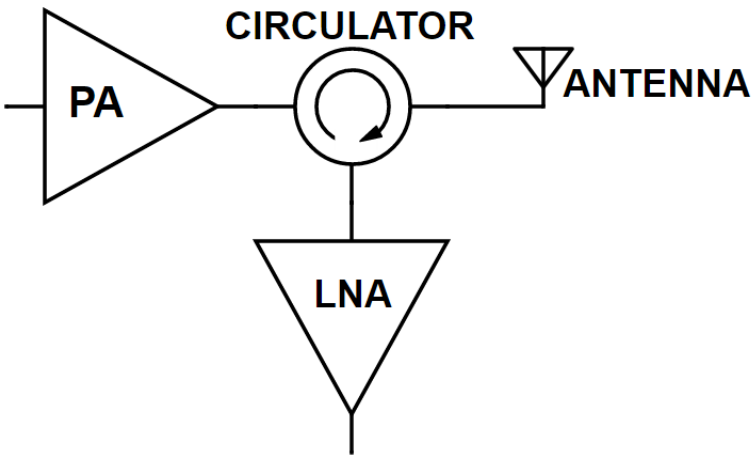

Figure 2.3: Circulator functioning as duplexer in a transceiver system

The protective function of isolator/circulator also find use in defense industry. Radar and other military communication systems usually have isolators at the receiver end to protect itself from maleficent outside EM jamming or internal TX leakage destroying the sensitive and costly receiver. This can be better illustrated in Figure 2.3

The schematic symbol of circulator and isolator are shown in Figure, where the arrow represents the circulating direction inside the device.

Besides being used as an isolator, another major use of the circulator is as a duplexer in transceiver front-end. It allows the transmitter and receiver to share a common antenna. It is also widely used in advance phased array radar systems to steer and shape the beam. It can provide isolation between transmitter and receiver from de-sensitization issue.

While designing a circulator, a designer should take into account the following parameters: [8]

- Operating frequency range
- Isolation
- Insertion loss
- Reflection in Voltage Standing Wave Ratio (VSWR)
- Power handling
- Operating temperature and self-heating
- Size and weight
- Linearity
- Types of transmission medium (coaxial, waveguide, microstrip line etc.)
- Shielding from external interference

Among all these parameters, isolation and insertion are the most concerning. Isolation indicates the separation of signal level from adjacent decoupled port, expressed in dB. Insertion loss is the

measure of how much energy is lost when transferring power from one port to the coupled port and it's also expressed in dB.

Size, weight and cost are other big concerns because as already mentioned in the first, a strong and uniform biasing magnet can be very cumbersome and sometimes it could even be the bottleneck of system integration. For example in a phased array radar system, there will be thousands of circulators to play role in beam forming. The size, weight and cost of all these circulators in total can be unimaginable if not well-controlled.

Operating temperature can sometimes be another serious issue. Permanent magnets usually set the upper limit temperature of operation for the whole device. The de-magnetized temperature for neodymium magnet is usually sixty to eighty degree centigrade. If we can achieve self-bias for ferrite material and get rid of the magnet, then this upper floor can be easily breached.

Considering all parameters and issues we discussed above, it's very attractive to make an on-chip and self-bias circulator that can solve all weight, size, cost and temperature limitation problems while keeping major specs like isolation and insertion loss uncompromised. It will be the final goal of this work.

2.2 Different Types of Circulator

Three ports circulators are the most common type of circulator since it can be easily used to replace "one pole two throws" switch or to terminate one port and use the other two as isolator. There are also enormous types of circulator available on the shelves, ranging from gigantic waveguide circulator used in a high power microwave system to the miniature on-chip integrated circulator that we are going to build. Different circulators have different size, weight and design but almost all of them share the same idea of phase manipulation, which will be clarified later.

Circulators are first categorized into active or passive groups. Passive circulators generally show superior performance comparing to their active counterpart, besides this work is passive so we will focus more on passive circulators. However it's worth mentioning that recently we see great performance improvement in insertion loss by a research group from Columbia University using no ferrite material, which is novel and promising. However their quasi-circulator can only operate below 1GHz and has many unsolved problems like low power handling and low solation. Passive circulators still dominates microwave frequency applications like at 60GHz.

Back to our topic of passive circulator. All passive circulators fall into these categories: Faraday rotation circulator, ring circulator, differential phase shift circulator, lump-constant circulator, junction circulator and field-displacement circulator and so forth. We categorized them into a tree map in Figure 2-4 so it's easy to trace. Among the family of passive circulator, junction circulator, lumped-constant circulator and faraday rotation circulator are the three most widely used models. We will cover them in detailed description below.

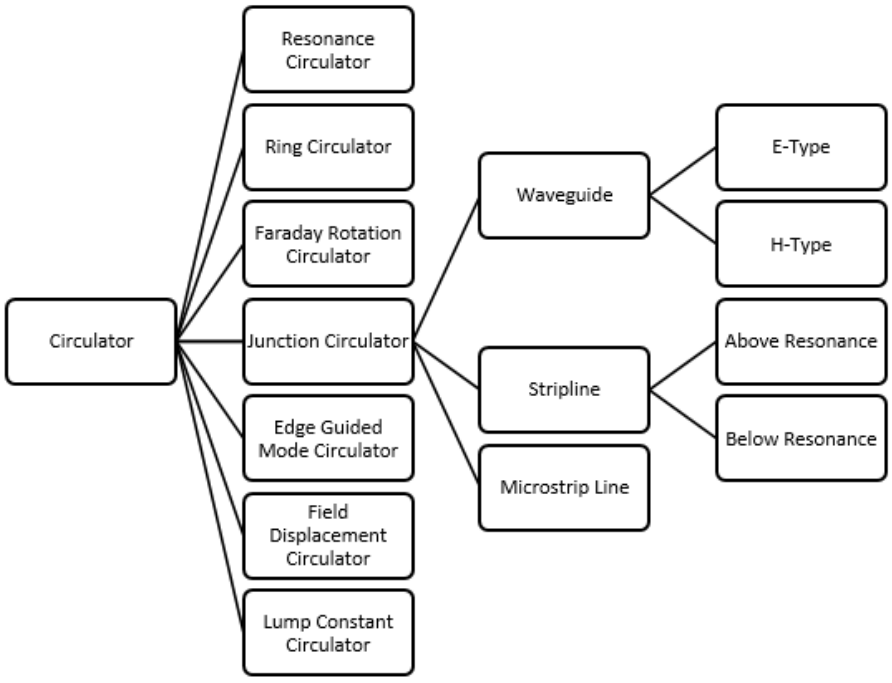

Figure 2.4: Different categories of circulator

2.2.1 Junction circulator

Among all types of circulator, the junction circulator is the most popular one due to the fact that it is usually compact and the design principle is already well-known to designers. Junction circulators are usually available in waveguide, stripline and microstrip line. The 3D model of a stripline junction circulator can be found in Figure 2.5. It is formed of ground plane, ferrite disk that provides magnetic biasing field and conductive stripline in sandwich structure. Usually junction circulators are implemented in a bottom-top mirrored structure with stripline in the middle and two magnets that provide stronger perpendicular field than single disk.

The center most conductor is in round shape that forms a resonator at given frequency. It's well-known that a linearly polarized wave can be decomposed into two circular polarized waves that have same traveling speed but opposite directions of polarization (one right-handed and left-handed circular polarized. If we remove the magnet, which means there is no biasing field present, signal enter port 1 and these two circular polarized waves will keep traveling at the same speed and form a standing wave as illustrate in Figure 2.6 (a). Power is evenly split in half and exits at port 2 and port 3. In this case it is functioning like a 3dB power splitter.

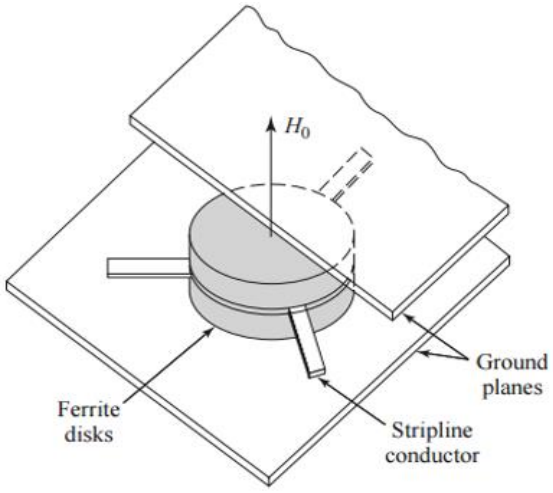

Figure 2.5: 3D model of stripline circulator [6]

With the help of the magnet and its biasing field, it becomes another story. The condition of equivalent propagating speed can no longer be met hence aforementioned two waves will sum up either constructively or destructively at specific distance from input reference plane. From the standing wave point of view, it will rotate by 30 degrees, either clockwise or counterclockwise, depending on the direction of bias field. If it rotates counterclockwise, the standing wave pattern will be as in Figure 2.6 (b), from which we can tell that resonated signal will be perfectly coupled to port 2 and exit while port 3 is "uncoupled". Or if the standing wave rotates clockwise, the similar case can be found in Figure 2.6 (c), but the difference is this time port 3 is coupled while port 2 is uncoupled.

In the ideal case the coupled port receives all signals from input and the uncoupled one is isolated from input. Since three ports are geometrically identical, if we feed signals into three ports at the same time, these signals will exist only from next ports to the right of it (or to the left of it in another bias field setting). And this is equivalent to signal circulating within three ports.

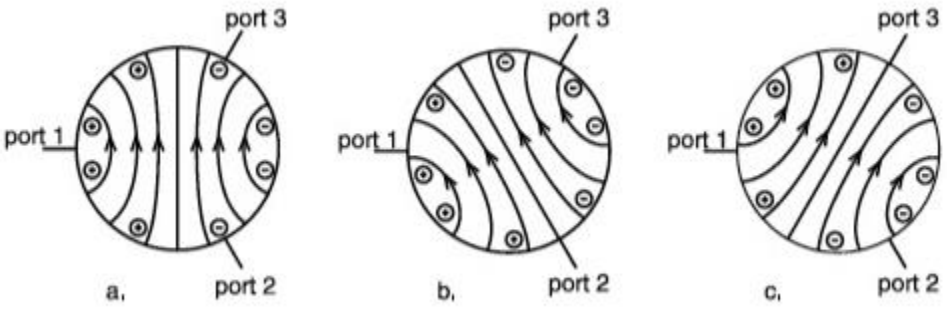

Figure 2.6: Standing wave inside operating circulator [7]

2.2.2 Differential Phase Shift Circulator

Differential phase shift circulator is another common type that is frequently used in applications that require high power handling capability. It is usually implemented in rectangular waveguides

because of the ease of construction. However comparing to the junction circulator, the insertion loss specs are usually higher.

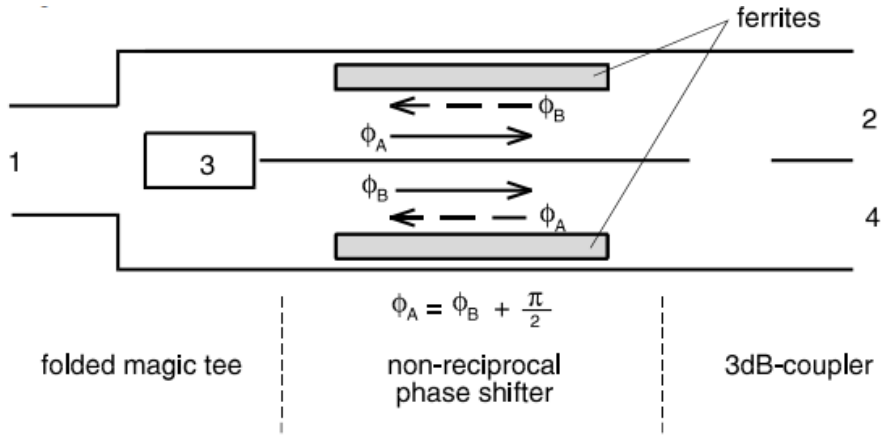

Figure 2.7 Structure of phase shift circulator [7]

There are mainly three building blocks of phase shift circulator a) a folded magic tee; b) a non-reciprocal phase shifter and c) a 3-dB coupler. The structure of circulator can be better illustrated in Figure 2.7. A wave entering port 1 will be evenly split passing the magic tee structure. These two waves have equal energy and phase. These two waves then propagate through the non-reciprocal phase shifter where in one path the wave is delayed by ψ_A and in the other path delayed by ψ_B where $\psi_A + \psi_B = 90°$. In the third section, a 3-dB coupler, both waves are split again into two equal parts but this time the split wave goes into other waveguide is delayed by 90°. Hence we will get two waves canceled at one port and add up at the other among ports 2 and port 3.

2.2.3 Faraday rotation circulator

It is not hard to tell from its name that the Faraday rotation circular is built based on the phenomenon of Faraday rotation, or Faraday Effect. It is a phenomenon of interaction between waves and magnetic field when the wave is propagating in a medium. The key effect of Faraday

rotation is, a wave travelling with a magnetic field in the same direction of propagation will experience rotation of polarization plane. Faraday rotation can be qualitatively explained as in Figure 2.8. Without the presence of magnetic field, two circular components are always equal in magnitude and opposed in phase hence along the y axis they always cancel each other. The polarization direction keeps aligned with that of the input wave during propagation. However if there is a magnetic field present, these two circular components still have the same magnitude but the phase equivalency in opposite sign doesn't hold anymore. That is to say the summation of these two components is going to gradually rotate along the direction of propagation.

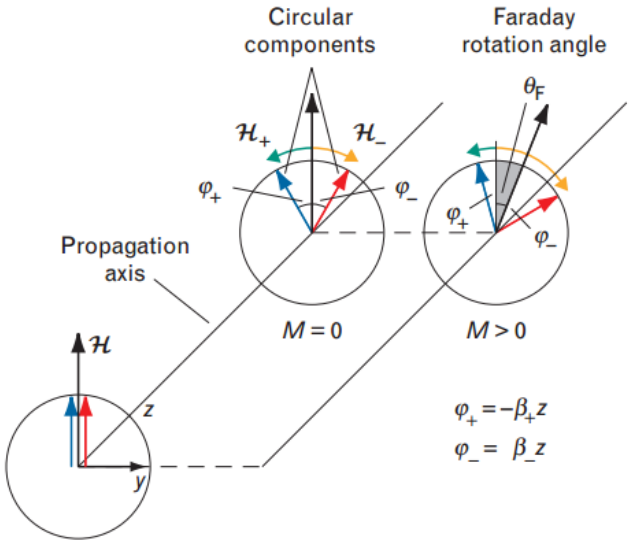

Figure 2.8 Schematic diagram of Faraday rotation in a ferrite magnetized medium [9]

Capturing the principle of Faraday rotation, a Faraday rotator can be easily built with a round waveguide and ferrite rod at the center. We can have 4 ports made of rectangular wave guide transition to circular waveguide in configuration as Figure 2.9 shows. Ports 2 and port 4 are made to be perpendicular to each other but both 45° to port 1 such that if the Faraday rotator is designed to provide another 45° rotation, the wave entering port 1 will be perpendicular to port 4 at output and only exit at port 2.

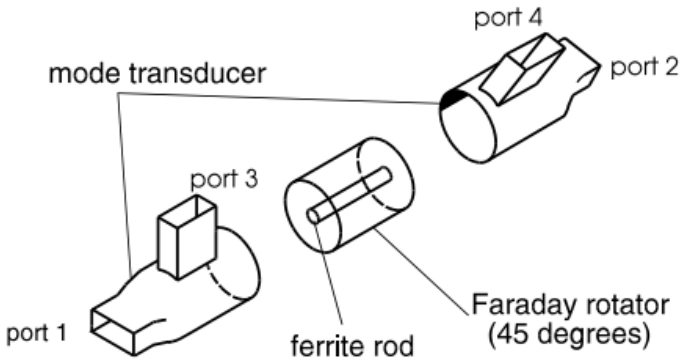

Figure 2.9 Schematic diagram of a Faraday rotation circulator [7]

2.3 Overview of Ferrite Magnetic Material

Magnetic phenomenona can be found in a group of oxide and semiconductors containing transition metal elements or rare earth elements that have unpaired electrons spin, or in another word magnetic moment, aligned. Depending on the situation of alignment, they can be categorized into four classes: paramagnetism, ferromagnetism, antiferromagnetism and ferrimagnetism.

Ferrimagnetism is only observed in complex compounds that have alignments of atoms at two different crystal sites under influence of exchange interaction. These two classes of site group into magnetic domains that present magnetic moment aligned but pointing to opposite direction. Within ferrimagnetic material one of them becomes major group and the overall net magnetic moment is not zero. Usually ferrites also come with high resistivity unlike ferromagnetic material, which is an attractive property to microwave and RF applications because it does not suffer from eddy current and related loss. [10]

Magnetic properties of ferrite materials differ from each other partly because of crystal structure differences. The exchange interaction is determined by the distance between cations and the overall

structural arrangement within crystallization. There exist mainly four types of ferrite materials exists. Below we discuss cubic, spinel, garnet and mostly important to this work, hexagonal ferrite.

2.3.1 Cubic ferrite

As perhaps the mostly widely used ferrite material, the well-known Alnicos cubic ferrite were developed in 1930s. It is an alloy of Al, Ni, Co and Fe and other elements in small amount. Because of its cation sites at vertex are equal in distance to each other, it is very stable regarding to temperature variation or demagnetization from shock or vibration. It finds itself in wide usage in motors and speakers in early days [10]. However the cubic ferrite exhibits low intrinsic coercivity which is part of the reason of undergoing replacement by hexagonal ferrite.

2.3.2 Spinel ferrite

Spinal ferrite is also in cubic frame but it is close packed cubic as in Figure 2.10. The chemical formula can be expressed in the general form of $MeO{\bullet}Fe_2O_3$ where Fe is trivalent and Me is a divalent metal like iron, manganese, copper, zinc, nickel and so forth. The exchange interaction between divalent and trivalent cations is the strongest among all cations. [10]

A worth-mentioning fact is the ferrous ferrite Fe_3O_4 spinel ferrite is the only type of ferrite that was discovered in nature. All other ferrites including aforementioned cubic ferrite, are manually fabricated. From the structure diagram, there are obvious two types of site for metal cations to live in. One octahedral site, which is surrounded by four oxygen ions, and another tetrahedral site which is surrounded by six oxygen ions. Note that not all sites are filled in a unit cell. The fact is these sites are loosely occupied. Only half of 32 octahedral sites and 8 out of 64 tetrahedral sites are occupied in spinel ferrite.

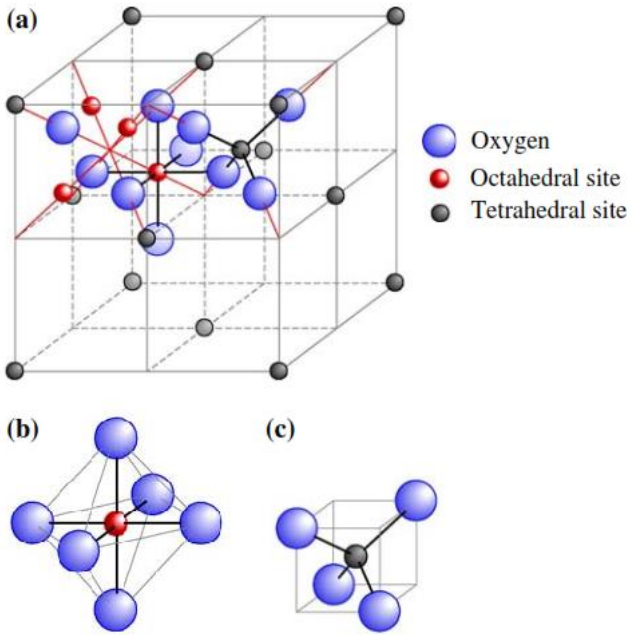

Figure 2.10 (a) Spinel unit cell structure (b) octahedral site and (c) tetrahedral site

2.3.3 Garnet ferrite

The crystal structure of Garnet is more complicated than spinel, which is orthorhombic. Besides octahedral and tetrahedral sites that can be found in spinel ferrite, there is a third site named dodecahedral which is a twelve-sided distorted polyhedral site. This site is usually occupied by a rare earth element instead of a common metal element. The magnetic moment of the rare earth element is not only determined by unpaired electron spin but also the orbital contribution of incomplete electron layers. One of the most famous garnet ferrites is Yttrium Iron Garnet (YIG), note that in YIG the Yttrium element don't even have spin contribution to overall magnetic moment. It features high Q value in microwave frequency and very small linewidth which is a measure of magnetic loss [11]. By substituting part of Yttrium ions in YIG with other types of rare earth element, the resonance frequency of ferrite can be shifted upward or downward. [12] These properties enable its usage in microwave ferrite devices like phase shifters and circulators.

2.3.4 Hexagonal ferrite

As the most important building block of this work, hexagonal ferrite is found in one of the most complicated structures. A unit cell of Barium hexagonal ferrite can be found in Figure 2.11

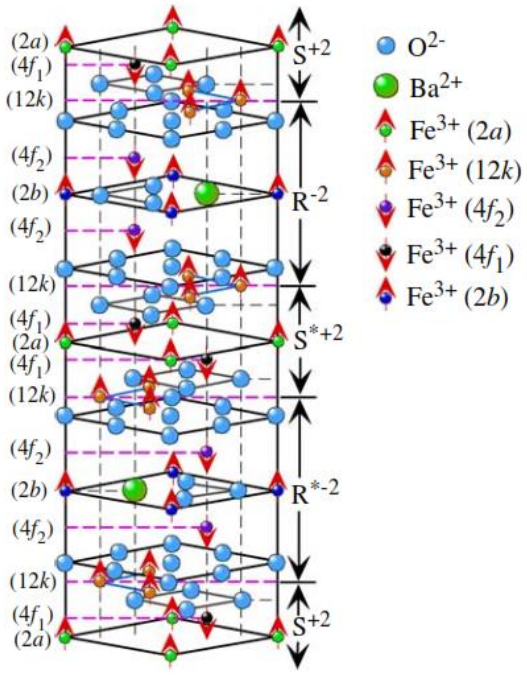

Figure 2.11 Unit cell of Barium hexagonal ferrite $BaFe_{12}O_{19}$ [10]

There is no general single formula that can include all types of hexagonal ferrite, but each type of hexagonal ferrite is interrelated. In Barium hexagonal ferrite for instance, the big barium cation which is shown in green in Figure 2.11, is the main cause of intrinsic anisotropic field. It also possesses other prevailing properties such as high saturation magnetization and ease to align the c-axis with external field. There are three subcategories of Barium ferrite: M-type, Y-type and Z-type, where Y-type and Z-type can be regarded as other elements substituted hybrid of M-type baseline. In our junction circulator design the M-type Barium hexagonal ferrite (BaM) is used for its highest magnetic properties among these three.

2.3 Overview of nanofabrication

Nanofabrication is the name of a group of fabrication techniques that sculpture miniature MEMS (Micro-Electrical and Mechanical System) and integrated IC out of sands (Si at the beginning and other compound substrate came out later). One of the merits of this work is the miniature size of circulator. Hence we need to employ some state-of-art nanofabrication to have it built from bottom to top. All types of nanofabrication processes more or less fall into three categories: patterning, deposition and etching. In the following paragraph, an introduction of several essential techniques from these three groups will be made and we can go through several special techniques that cannot be categorized into any of these groups. But let us visit the mostly important process of nanofabrication among all: photolithography as patterning techniques.

2.3.1 Photolithography

The reason why photolithography is the most essential nanofabrication technique is it enable us to define patterns and by adding and subtracting different patterns of material, we can build incredibly complicated structures at nanoscale. The key of photolithography is the material named photoresist.

Photoresist is a family of light-sensitive materials that change their own solubility to specific solvents under exposure of light in a range of wavelengths [13].There are also resists exposed by electron beam developed recently but is beyond the scope of this work. Ordinary photoresist use ultra-violet (UV) light for exposure and an area that is exposed to UV light becomes much more (or much less) soluble in developer, which is organic solvent. If we masked light with pre-defined pattern then such pattern can be transferred to a photoresist layer and developed. There are two polarities of photoresist, the one which becomes more soluble after exposure is positive photoresist and the opposite case is negative photoresist. The resolution of exposure is generally proportional

to the wavelength of light that is used. Figure 2.11 illustrates a standard photolithography process consisting of coating, exposure and developing and the following etching process that transfers the pattern from photoresist to the layer underneath.

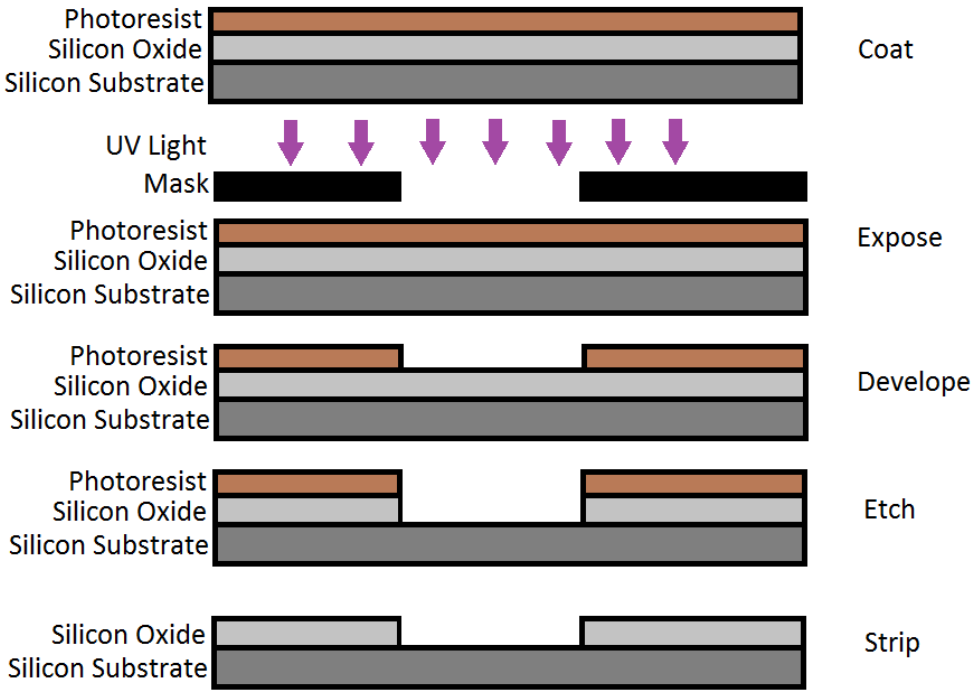

Figure 2.11 Processes of photolithography and pattern transferring

The patterned photoresist layer is both physically and chemically stable and can be used as a mask for underneath layer etching or as a sacrificial layer for lift-off process. Another issue of photolithography is when fabricating multi-layers structure there are normally one or more than one mask for each layer that needs patterning. All these masks need to be aligned with each other so that vertical structure does not skew and cause device failure.

There are two main resolution specs we need to consider in photolithography:

a) Features resolution: The smallest aspect ratio of finest structure is limited by the wave length of UV light. The most modern lithography is employing Deep UV and Ultra-UV light to shrink channel length of VLSI down to 7nm. In our application the smallest feature is at micron scale so normal UV exposer can meet our need.

b) Alignment resolution: In reality any feature on top of another cannot be placed at the wanted location with perfect precision. This is limited by the aligner tool and operator. In some applications the alignment mismatch can cause a critical effect on performance or even failure. Mask designers need to take it into consideration when designing multilayer masks. In this design we enlarged some features in one of the masks according to the typical mismatch of available aligner thus that bottom feature can be covered.

2.3.2 Deposition Techniques

Nanofabrication in conclusive words is addition and subtraction of patterned layers. Deposition is an addition process that can deposit either crystalized or composite material thin film on given surface. Due to the stringent requirement on the purity of deposited thin film, all following depositions happen in a high vacuum chamber or pure background gas atmosphere. According to the principle of material growth, deposition processes can be grouped into two types: physical deposition and chemical deposition.

Physical deposition includes sputtering, evaporation, atomic layer deposition, Pulsed Laser deposition.

a) Sputtering

As widely used to deposit metal, alloy and oxide, sputtering is perhaps the most equipped thin film physical deposition system. Its principle of operation is to employ Argon ion plasma that

is usually generated and sustained by a radio frequency source to accelerate and hit a pure target material ingot in electrical field and physically blast and sputter them onto wafer [14].

b) Thermal evaporation

Thermal evaporation is usually employed to deposit common metal or alloy. But the option of metals is limited by their evaporation temperature. This is derived from the principle of TE system is to feed large current through tungsten boat that holds target metal pellets. Temperature of the boat is going to rise above the metal boiling temperature and vapor of the metal will rise and deposit on the wafer that is installed facing down.

c) Electron beam evaporation

E-beam evaporation is the sibling of thermal evaporation which employs an electron beam focused on and heating target material to evaporate. The focus location is controlled by magnetic field and current of electron beam. E-beam heats up much quicker than its thermal counterpart but the heating process is less uniform. This fact will cause uneven expansion and cracking in some metal which influences the quality of deposited film.

d) Pulsed laser deposition

Pulsed laser deposition is similar to E-beam but instead of using electron beam, PLD employs a high power pulsed laser to ablate target material and create plasma during the pulse. The plasma then moves to the surface and nucleates into thin film.

Chemical deposition uses either precursor gases or solvents to transport material needed for chemical reaction at the surface. They include but not are limited to Chemical Vapor Deposition (CVD), different phases of epitaxy and so forth.

a) Chemical Vapor Deposition

Chemical vapor deposition is implemented by feeding one or more precursor gases into the chamber and imposing high temperature and high pressure to the wafer surface. Chemical reaction of precursor gases happens on the surface and solid film of mono-crystal, poly-crystal, amorphous and polymer can be deposited. The reaction rate can be greatly enhanced with help of plasma, which is named as Plasma Enhanced CVD (PECVD) [15].

b) Epitaxy

Epitaxy of thin film can happen in vapor, liquid or solid phase. Vapor phase epitaxy is a modification of chemical vapor deposition and is usually used to deposit doped silicon layers. Liquid phase epitaxy is a method of growing semiconductor material from melt of carrier material with target material dissolved inside. The temperature of LPE is critical to quality of film and this is a relatively fast method of thin film growing. There is also a molecular beam epitaxy (MBE) technique that finds application in III/V semiconductors growth [16].

2.3.3 Etching

After we deposit a layer of material and coated with patterned photoresist, the issue is now how to remove unwanted area. This is usually done by etching. Etching methods are also twofold: wet etch and dry etch.

Wet etch is a method to use acid or etchant to remove specific layer of material. The reaction rate of wet etch is much higher than dry etch and is difficult to control. Since the whole wafer needs to be soaked in etchant, any open surface will expose. Hence the compatibility of existing features material with etchant is a huge concern. Every etchant shows etching selectivity toward one or more material, but that is not saying material with low selectivity is guaranteed safe in this etchant. It is only a measure of low reaction rate.

Dry etch, on the other hand, is an elaborate method that features controllable etch rate and less compatibility issues comparing to wet etch. As an example, Reactive Ion Etch (RIE) is a modification of aforementioned Chemical Vapor Deposition. The difference is precursor gas used for deposition, for example Silane gas for silicon oxide deposition, is replaced by fluoride or chloride gas that can attack material. The etching speed can be well-controlled by tuning precursor gases intake rates and reaction conditions. It enables fine sculpture of layer thickness, which is crucial in some situations.

2.4 Review of Barium Hexagonal Ferrite Film Deposition Techniques

It is explicit that ferrite film deposition is a special sub-category of standard film deposition introduced in last section. However because of the complexity of crystal structure of ferrite like hexagonal type ferrite, the deposition of such materials are the elaboration of existing techniques and there are also some uncommon process that we'd like to go through.

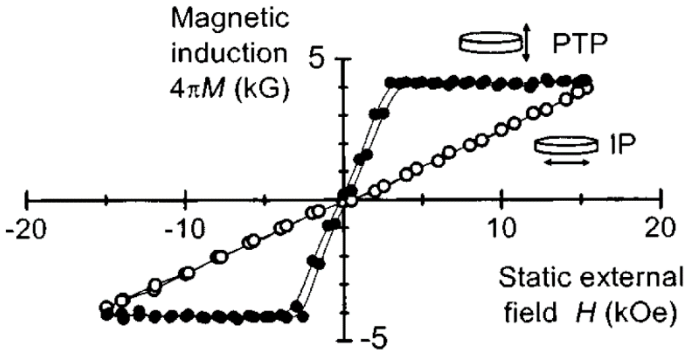

Figure 2.12 Hysteresis loop of PLD deposited BaM ferrite thin film with static external field applied perpendicular to plane (PTP) and in plane (IP) [20]

The best candidate of Barium hexagonal ferrite thin film for ferrite devices should features strong saturation and remnant magnetization, narrow ferromagnetic resonance linewidth, large dielectric constant and good mechanical properties [17]. Various types of deposition techniques have been proposed and experimented [18-25]. They are listed as sputtering [18], pulsed laser deposition [20], Alternating Target Laser Ablation Deposition (ATLAD) [21], Liquid Phase Epitaxy [22], screen printing [24] and ferrite composite spin casting [25] and so forth.

Among the best quality BaM films with c-axis perpendicular to film plane made by PLD are those reported by Song et al [20].The magnetic hysteresis loop is shown as in Figure 2.12. Their films have resonance linewidth as small as 16 Oe at 60 GHz and large anisotropy field and saturation magnetization. However the remnant magnetization was quite small and the film thickness is limited to 0.85um because of excessive stress. Hysteresis loop results of their film is shown as in Figure 12. Among thicker BaM films made by LPE or hybrid PLD/LPE technique, the best result is also as reported by Song et al [22]. They deposited a thin seed layer of BaM by PLD, then grew a second layer up to 45 um upon it by LPE. VSM measurement indicates a linewidth of 40-68 Oe. However the near-zero remanence ratio Mr/Ms (RR) indicates its inability to achieve out-of-plane self-bias. Song's result shows in-plane c-axis orientation can be achieved but for out-of-plane this is not the case. On the other hand, techniques such as screen printing [24-25] and spin-casting that employ Micro or Nano powder have out-of-plane self-bias properties with high RR in the range of 0.7-0.95 but the down side of such techniques is the wide resonance linewidth (i.e. loss in material), usually in 300-500 Oe range.

2.5 60GHz Unlicensed Frequency Band

Next generation wireless communication systems requires the capability of multi-gigabit speed as traditional wireless gateways following standard 802.11a/b/g (2.4GHz) and 802.11n (5GHz)

cannot meet future needs of high speed wireless applications. 802.11g provides up to 54Mbps at 2.4 GHz and 802.11n provides up to 100 Mbps at 5GHz with Multi-Input Multi-Out implementation. The target data rate at 60GHz is however above 1 Gbps. Researchers are now focusing on millimeter wave frequency band up to 60 GHz for potential solution. One of the facts about 60GHz is the atmospheric absorption in this frequency range is very high. International Telecommunication Union published the atmospheric data as in Figure 2.13.

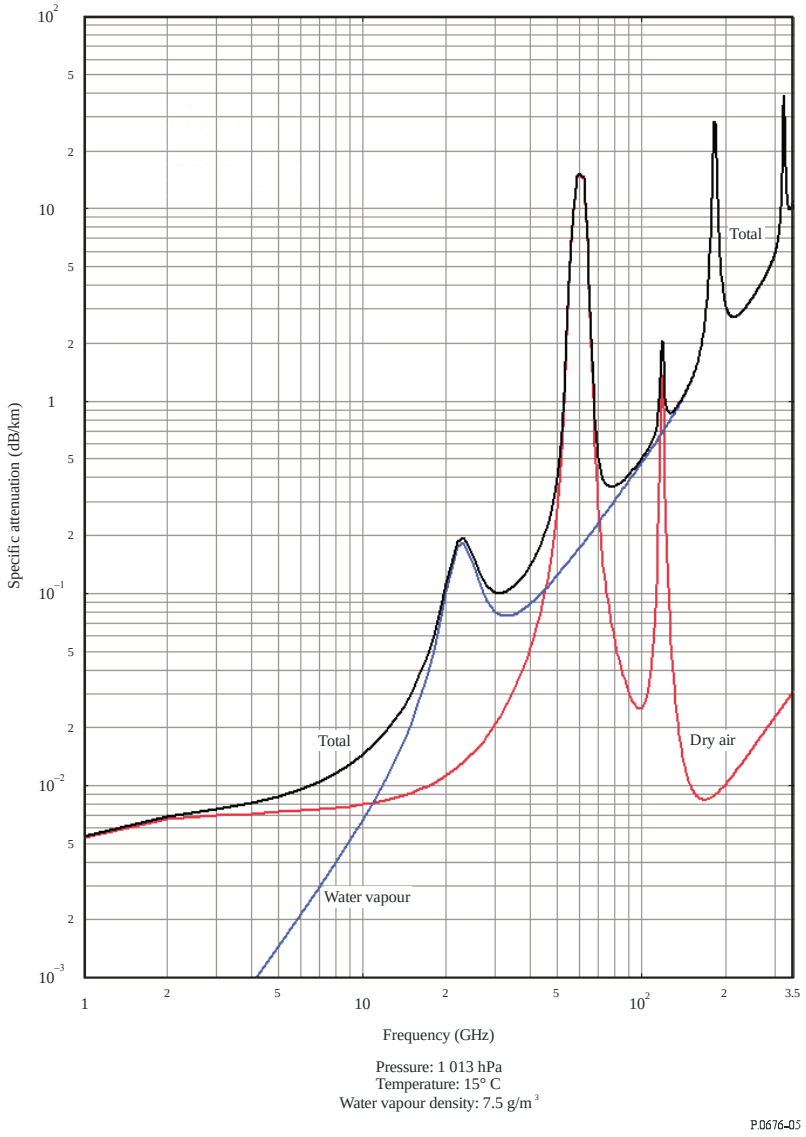

Figure 2.13 Atmospheric attenuation spectrum of free space propagation [26]

Note that at 60GHz the main attenuation factor in air is Oxygen instead of water vapor. High absorption at 60GHz is advantageous since it limits the cover distance thus interference of a neighboring access point is minimized and frequency re-use is easier, which is crucial to multi-user system. The US Federal Communication Commission devoted frequency 57GHz-64GHz for unlicensed application in 2001 [27] and is incentive to development of 60Ghz applications since then.

At 60GHz, the circulator as a main building block of front-end modules, is of significant use to high speed wireless communication.

Chapter 3 Characterization of hexagonal ferrite

Key performances of a circulator including operating frequency, bandwidth, insertion loss and power and thermal handling are directly determined by the properties of selected ferrite material. In this chapter, we introduce the characterization of ferrite material employing free-space quasi-optic spectroscopy in Professor Afsar's laboratory. The measured properties includes some of the key parameters we utilized in full-EM simulation, which we will cover in Chapter 4.

3.1 Free-space quasi-optic spectroscopy system

Free space quasi-optic spectroscopy, a powerful non-destructive measurement technique in microwave and millimeter wave frequency range, has been well studied and successfully employed [28]. Measurement of complex permittivity and permeability of numbers of various samples has

been implemented and presented by several researchers [29 and 30]. Source of this quasi-optic spectrometer is three high-vacuum, high-power backward wave oscillators (BWO) tunable in Q, V and W bands respectively. These three bands cover the frequency range from 30 to 120 GHz. A propagation path is set up by using a couple of pyramidal horn antennas and polyethylene made lenses. Antenna and lenses are well aligned and adjusted to form a Gaussian beam focusing on the sample. Transmitter and receiver are placed on opposite side of sample and the schematic diagrams of the system are shown in Figure 3.1.

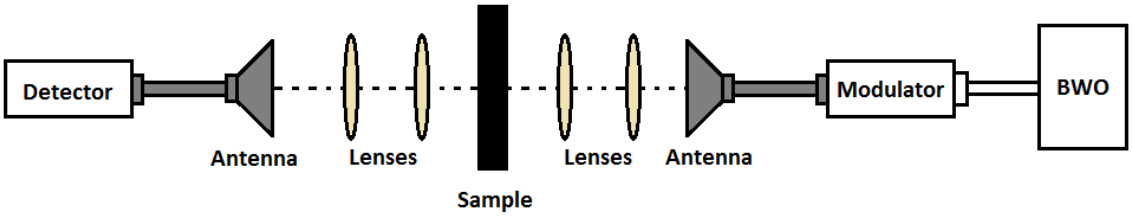

Figure 3.1 Schematic of setup of free space quasi-optic spectrometer with Backward Wave Oscillator (BWO) source

Figure 3.2 Picture of free-space quasi-optic spectrometer in millimeter wave frequency

The normalized transmittance of all ferrite samples show an obvious absorption notch at different frequency. This derives from the phenomenon of Larmor precession which is the precession movement of magnetic moment of magnetic domain with or without external field. If we applied an EM microwave perpendicular to the external field, the ferrite become increasingly absorptive as microwave frequency approaching precession frequency and the highest absorption frequency is also known as resonance frequency. This results in two circulator operation types: Above Resonance (AR) and Below Resonance (BR) circulator if the resonance frequency is above or below the operating frequency.

From the absorption spectra we can also calculate the complex permittivity and permeability of sample. Complex permittivity of a flat parallel slab or thick film of sample can be determined by investigating the amplitude change of transmittance spectra together with phase change during wave propagation in sample media. The well-known equations [31] are shown as below:

$$T = E\frac{(1-R)^2 + 4Rsin^2\psi}{(1-RE)^2 + 4REsin^2(\alpha+\psi)},$$

$$R = \frac{(n-1)^2 + k^2}{((n+1)^2 + k^2)},$$

$$\varphi = \alpha + \tan^{-1}\frac{ERsin^2(\alpha+\psi)}{1-ERcos^2(\alpha+\psi)} + \tan^{-1}\frac{k}{n^2+k^2+n} - \tan^{-1}\frac{k}{n+1}$$

$$E = e^{-4\pi kdf/c}, \qquad \alpha = \frac{2\pi ndf}{c}, \qquad n + ik = \sqrt{\varepsilon^*\mu^*}$$

$$\psi = \tan^{-1}\frac{2k}{n^2+k^2-1},$$

where *T*, *R*, *n* and *k* are transmittance spectra, reflectance spectra, refractive index and absorption index respectively. Complex permittivity and permeability are ε and μ, c is the speed of light, φ is the phase of the transmitted wave and ψ is the phase of reflected wave.

From the expression we learn that amplitude of electromagnetic wave transmitted through a dielectric layer is an oscillating function of sweeping source frequency. Each time when $\alpha + \psi = \pi l$, where l is integer, transmittance response reaches a peak. By inspecting the distance of frequency between two neighbor local maxima in transmittance spectra, we could evaluate refractive index. Absorption index, which is responsible for the attenuation, is closely relevant to the change of amplitude. Both refractive index *n* and absorption index *k* can be determined by a curve fitting procedure.

Unlike non-magnetic materials, whose permeability is very close to unity and change at high frequency can be dismissed, materials with strong magnetization show changes across broad frequency that cannot be ignored.

To evaluate the complex permeability of Barium nanoferrite, we employed Schlömann's equation [32] for partially magnetized ferrite material:

$$\mu_{eff} = \frac{1}{3} + \frac{2}{3}\sqrt{\frac{(H_A + 4\pi M_S)^2 - \left(\frac{\omega}{\gamma}\right)^2}{H_A^2 - \left(\frac{\omega}{\gamma}\right)^2}},$$

where ω is the frequency, H_A is anisotropy field, $4\pi M_s$ is saturation magnetization, γ is gyromagnetic ratio. From ferromagnetic resonance we could determine anisotropic field and saturation magnetization. Gyromagnetic ratio can be expressed as:

$$\gamma = \frac{ge}{2mc},$$

where g is Lande factor approximately equal to 2. After changing the unit we have the gyromagnetic ratio of electron equal to 2.8 GHz/kOe.

3.2 Characterization of hexagonal nano-ferrite and composite

Prior to this work, there is a thorough study of complex permeability and permittivity of micro-size and nano-size hexagonal Barium ferrite ($BaFe_{12}O_{19}$) and Strontium ferrite ($SrFe_{12}O_{19}$) that is conducted by colleagues of our research group [25]. The author of this thesis also performed similar study on the mixture of ferrite and polymer in broadband millimeter wave frequency range. Strontium and Barium ferrite powder were ordered from American Elements. The product numbers of Strontium and Barium are SRFE-OX-02-NP 99% and BAFE-OX-02-NP 99% respectively. The average size of powder is 60nm, which is already smaller than the average size of magnetic domain. Each powder can be regarded as quasi-monocrystalline that has magnetic domain aligned within itself. This is advantageous in achieving self-bias, which will be covered in the next Chapter.

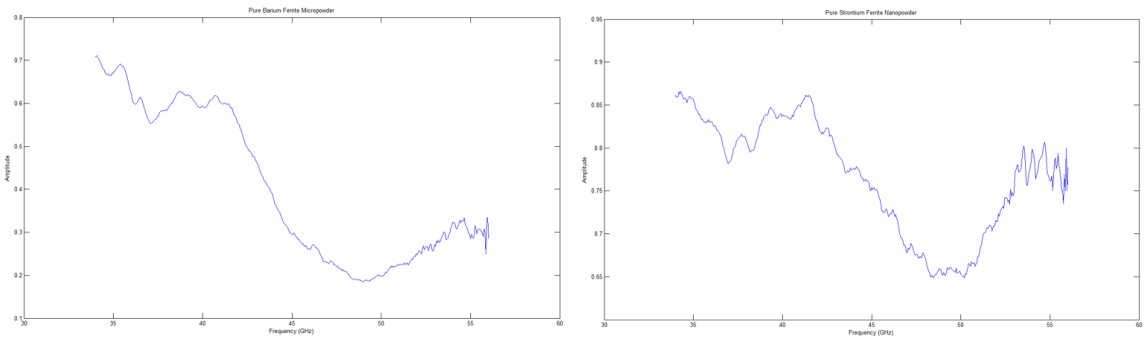

Figure 3.2 Transmittance of hexagonal Barium (Left) and Strontium (right) nanopowder

Employing the free-space quasi-optic method, the transmittance data in Q, V and W bands is shown in Figure 3.2. The resonance frequency of Barium nanopowder is 47 GHz and for Strontium nanopowder it is 51 GHz. By employing measurement and computation methods introduced in last section, we can tabulate Table I with a summary of Barium nanopowder.

A preliminary study conducted by collaborator and Prof. Afsar's group shows the influence of mixing ferrite nanopowder and polymer such as photoresist on the resonance frequency of prepared sample. But what is revealing about this composite is the possibility of employing spin casting to deposit nanocomposite material at low temperature [25]. Hence beside pure ferrite nanopowder, the author of this thesis also characterized composite of Barium ferrite nanopowder with photoresist and compared them with pure powder.

The preparation of composite sample is implemented as follow:

1. Set up scale and hot plate in fume hood. Put an empty cup on scale and recalibrate it as zero reference. Set temperature of hot plate at 110 degree Celsius.
2. Slowly add photoresist AZ9260 into cup using pipette
3. Add a small amount of barium nanopowder using sample scoop and stir the mixture until there is no visible powder on surface.
4. Keep adding nanopowder and repeat step 3 until the mass ratio of photoresist and ferrite powder reach 1.
5. Stir composite non-stop for 5 minutes then pour it into a 3 inches Polystyrene Petri dishes and leave it in fume hood for 30 minutes so it reflows into a flat surface.
6. Bake it on hot plate until sample is completely hardened

The reference of transmittance measurement of this sample will be an empty Polystyrene Petri dish so its influence can be de-embedded. The transmittance data of composite data is shown in

Figure 3.3 and it shows identical resonance frequency to pure powder but we can tell the difference by using Schlömann's equation to calculate the complex permeability of composite and the results are shown in Figure 3.4

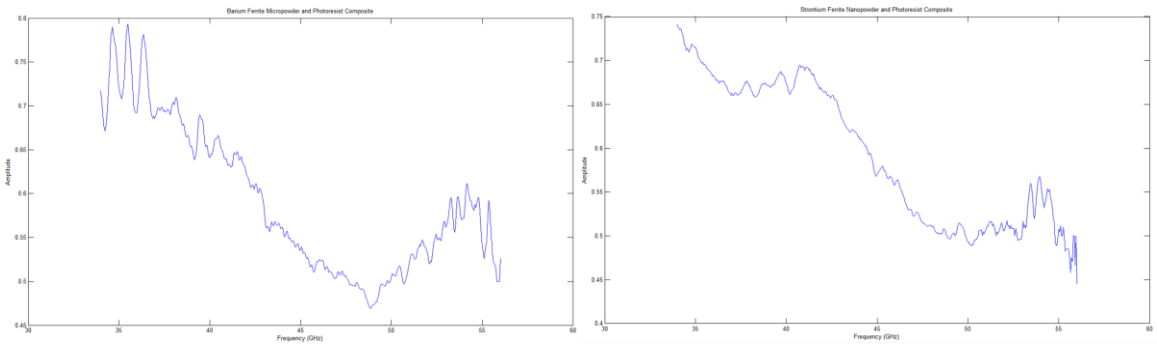

Figure 3.3 Transmittance of hexagonal Barium nanoferrite composite (left) and hexagonal Strontium nanoferrite composite

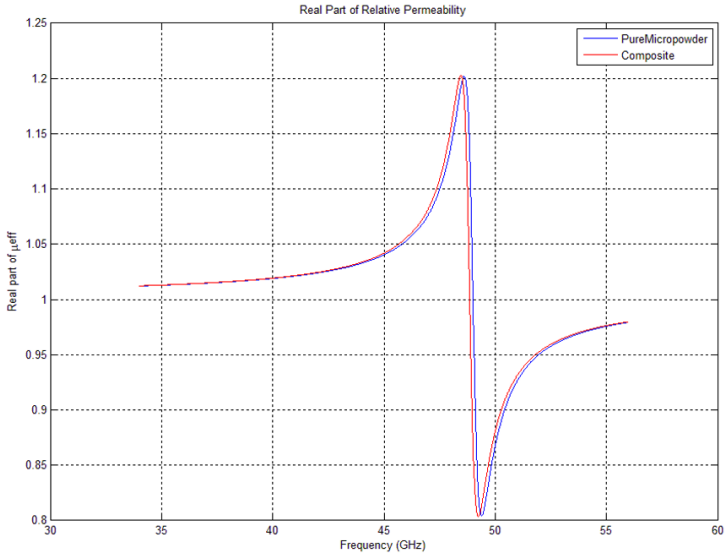

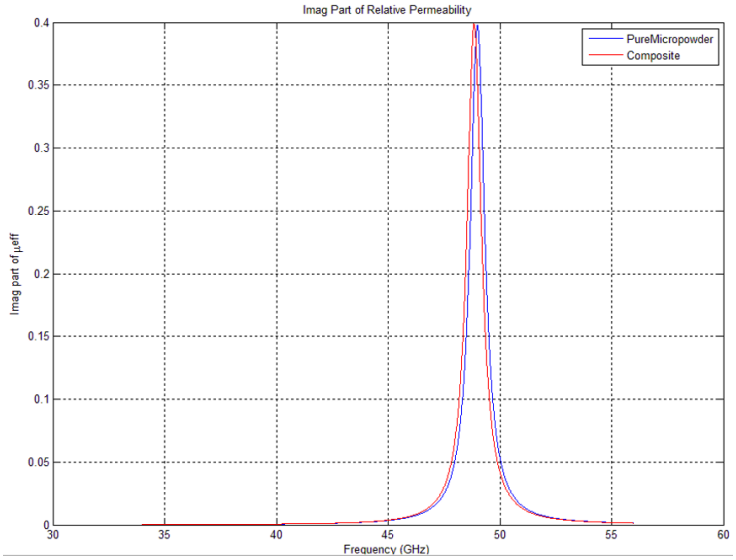

Figure 3.3 Real (Top) and Imaginary (Bottom) part of Permeability of hexagonal Barium ferrite composite and pure Barium ferrite nanopowder

Note that the resonance frequency of hexagonal Barium ferrite composite is slightly lower than pure powder. However the difference is very minor and the root cause of this phenomenon can the isolation effect of polymer on the coupling between powders.

Besides permeability data, as introduced in last section, we can measure and calculate the complex permittivity from transmittance data as well. A summary of hexagonal Barium ferrite composite is presented as in Table I.

TABLE I: PROPERTIES OF BARIUM FERRITE COMPOSITE FILM

Name	**Value**	**Unit**
Resonant Frequency	45.5	GHz
Anisotropic Field	16.25	kOe
Resonant Linewidth	2.8	kOe
Refractive Index	2.06	
Absorption Index	0.04	
Real Permittivity	4.24	
Imaginary Permittivity	0.16	

Gyromagnetic ratio is 2.8 GHz/kOe

3.3 Study of thermal annealing on ferrite film on GaN-on-SiC substrate

All ferromagnetic materials have losses that damp out around resonance, where damping force resist the precessional movement and tend to relax into equilibrium. Such loss is denoted by the ferromagnetic resonance linewidth. Linewidth. It is the converted half-peak width of imaginary permeability or the peak to peak width of real part of permeability in the unite of Oersted. Typical linewidth of ferrite material ranging from as narrow as one Oersted in monocrystalline YIG ferrite with good quality to hundreds or thousands of Oersted as in composite ferrite.

It is known to researcher that high temperature treatment can narrow the linewidth by either recrystallizing amorphous material to release internal stress, or by burning out binder material in metallurgy method deposit ferrite to increase the percentage of ferrite and reconfigure grain boundary. In order to investigate the influence of high temperature heat treatment on the property of composite film, one issue that needs to be resolve is the compatibility of substrate. Silicon substrate, as used in CMOS technology, cannot withstand temperature more than 200°C. Above this temperature the performance of CMOS circuit will be greatly degraded. Other common III/V group compound substrate faces the same issue. This is limited by the narrow bandgap of substrate material [34]. Nevertheless there has been few relatively little research on ferrite material on Gallium Nitride, which is wide bandgap material that is able to withstand 900°C [35].

Four inches GaN-on-SiC wafers are provided by Qorvo Inc. in Texas. Thickness is 2 um and 500 um for GaN and SiC respectively. In order to make more test and for the convenience of sample loading, each 4'' wafer was diced into 4 fan-shape chips, and are able to fully cover the sample loading hole, where the beam waist of Gaussian wave will penetrate through sample, which is 1.5'' in diameter.

Ferrite composite is made of nanopowder and photoresist AZ9260 with mass ratio 1:1, which

possess the highest percentage of ferrite powder that we could apply spin-casting to. The paste was well mixed by using a vortex mixer. It was spin-casted onto GaN-on-SiC substrate and baked on hotplate. A Neodymium magnet with residue induction $Br_{max} = 13400$ Gauss was used during baking to provide biasing field with direction perpendicular to substrate plane. After baking the thickness of ferrite film is 3mm thick. As a reference, pure ferrite nanopowder was loaded into a special-made container. The powder chunk was 5mm in thickness.

Figure 3.4 Photos of Muffle furnace employed for high temperature heat processing

To study to influence of heat treatment on film quality, 3 samples were prepared and heated in chamber separately for one hour. Heat treatments were implemented in atmosphere at 300°C, 600°C and 900°C. The Muffle furnace was ordered from Certified Material Testing Product with product number BCL-705 featuring maximum temperature 1260 degree Celsius. In Figure 3.4 is a picture of furnace.

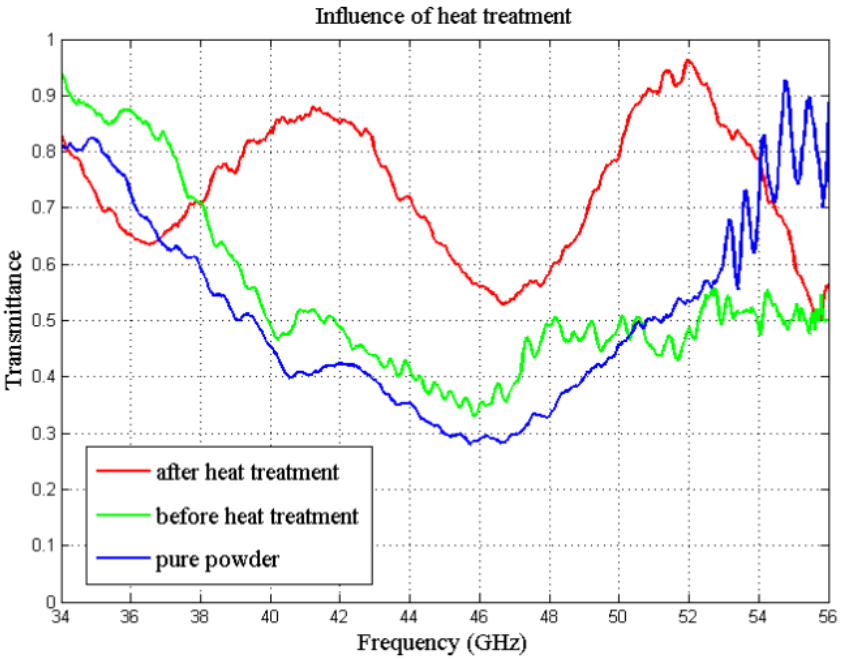

Figure 3.4 Transmittance of pure barium ferrite powder, ferrite composite before and after heat treatment at 600°C

Processed films were measured using quasi-optic spectrometer like aforementioned non-heated samples. Out of three temperature condition, sample processed at 600°C shows the narrowest FMR linewidth. The transmittance plot of pure powder, composite and composite processed at 600° is in Figure 3.4 and the complex permeability plot is in Figure 3.5.

Comparing to unprocessed sample, heat treatment shortened resonant linewidth from 2.8 kOe to 1.7 kOe. However the film became porous after polymer was partially burned out and shrunk, which is the bottleneck to its integration and application. But we see the potential of heat treatment to further improve resonant linewidth if we make film with higher ferrite density and homogeneity. The characterization of GaN/SiC substrate was also implemented. Complex permittivity and permeability are obtained following the same procedure. The derived complex permittivity and refractive index are shown as follows in Figure 3.6

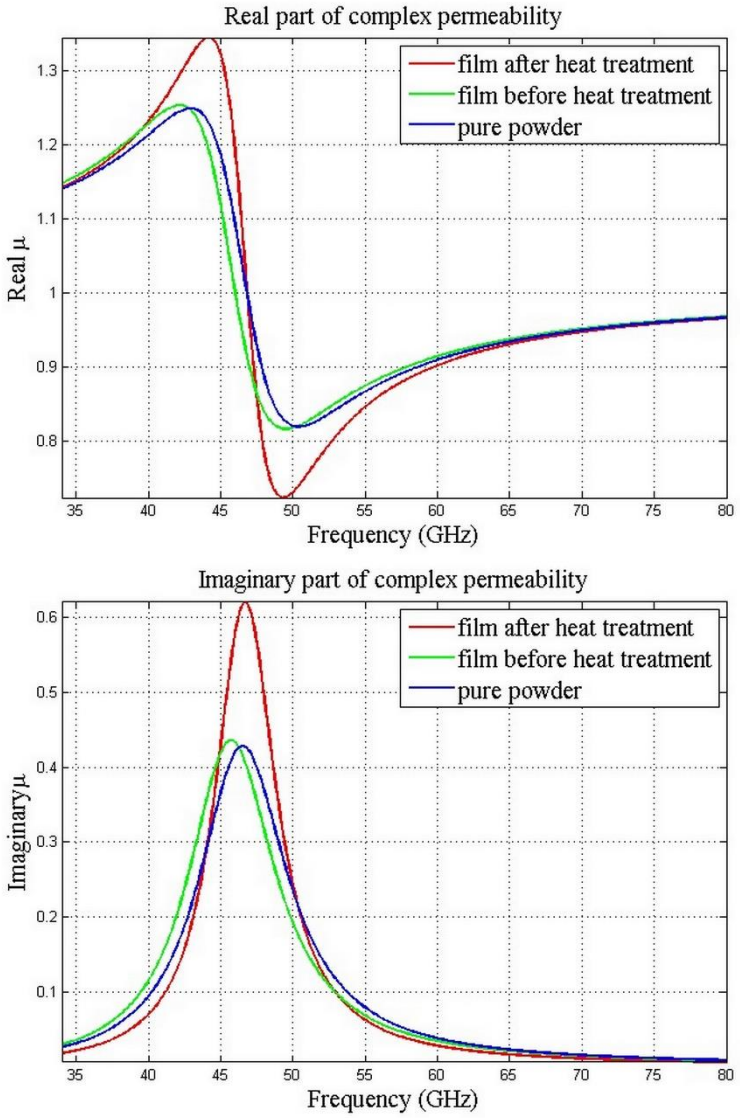

Figure 3.5 Real (Top) and imaginary (bottom) part of permeability of pure powder,

The averaged permittivity of GaN/SiC substrate in the Q band is close to the result of permittivity of bare SiC substrate presented by Shu Chen et al [36], but the variation is higher than their results. This is partly caused by the two layer structure of the sample since the interface between GaN and SiC layers induces more error. Our permittivity measurement of ferrite film is more accurate because GaN/SiC influence is de-embedded from result as reference hence measurement is conducted on ferrite film itself. However the measurement of GaN/SiC with air reference cannot

dismiss this factor. To further improve the accuracy of permittivity measurement, we could use a bare SiC substrate as reference.

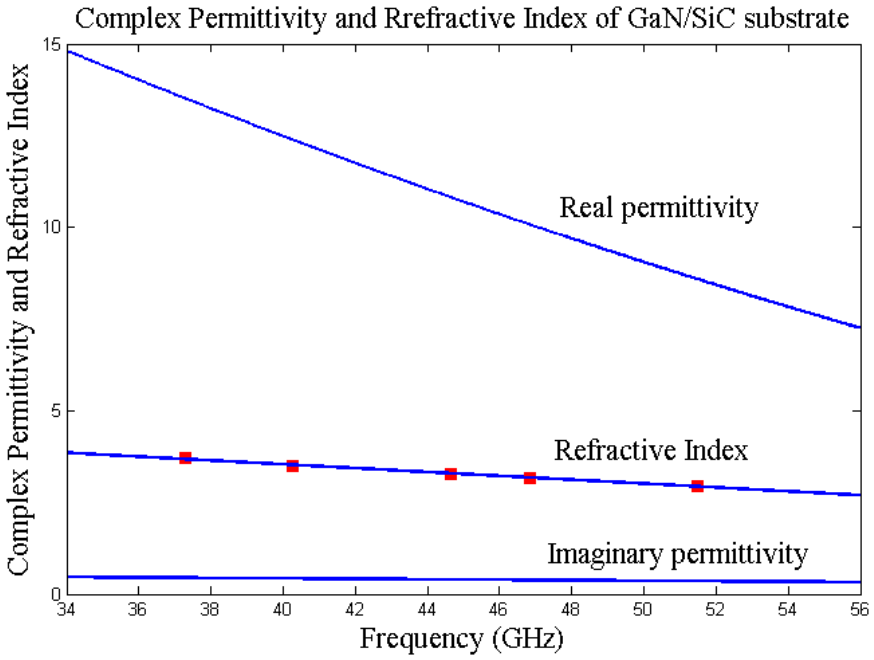

Figure 3.6 Complex permeability and refractive index of GaN-on-SiC over air reference in Q band

Chapter 4 Design, simulation and fabrication of ferrite circulator

4.1 Overview of transceiver front end module

Transceiver is the name of a module that includes both transmitter and receiver. These two paths share one antenna for both uplink and downlink because antenna takes much more room or area on chip to fabricate. Antenna sharing is a strategy that makes product competitive in both size and cost. The drawback of antenna sharing also very explicit: power amplifier in transmitter path, which values efficiency and power specifications the most, will interfere with receiver path low noise amplifier, which values noise level and sensitivity the most. Inter-module interference that lowers the sensitivity of receiver is called de-sense. In modern integrated front-end module, isolation has become one of the most important specifications that designers should give careful consideration to.

There are generally two ways of duplexing strategy in two different domain: time domain duplexing (TDD) and frequency domain duplexing (FDD). For instance there are two version of LTEs: LTE TDD and LTE FDD. The idea of TDD is to divide operation into narrow time slot and by employing a high speed single throw-two pole switch to assign the usage of the antenna to either transmitter or receiver. The switching frequency should meet at least the sampling frequency of uplink and downlink data. FDD on the other hand, enable continuous signal transmitting and

receiving at the same time, but they are assigned to different band frequencies in frequency domain, in that way they don't interfere with each other.

Circulator plays the role of frequency domain duplexing in front-end module as illustrated in the system diagram in Figure 4.1.

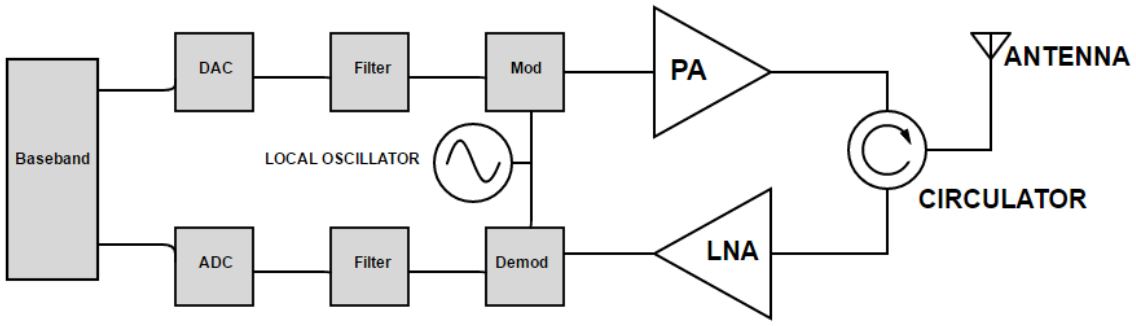

Figure 4.1 Schematic diagram of amplitude modulation front end with circulator as duplexer

This is a simple amplitude modulation (AM) system in direct conversion architecture. In the transmitter path, from left to right, baseband signals generated by the baseband signal processor are converted from digital to analog signal then low pass filtered to remove unwanted harmonic produced by the digital-to-analog converter (DAC). This analog baseband is then modulated by local oscillator (LO) up to RF frequency and gains power from the power amplifier. Such high power signal is then fed into the circulator with antenna connected to the full transmission port so it can transmit via antenna with lowest loss.

In the receiver path, from right to left, signal received by the antenna will be directly fed into the circulator. Because the circulator is a non-reciprocal device, the full transmission path from PA to antenna now reversely behaves as an isolated port, and the full transmission path is the one the low noise amplifier connects to. The low noise amplifier should amplify the signal with minimum noise

because it's the very first stage of receiver path and according to the noise figure equation of a cascaded system, the noise figure of the first stage directly adds onto system noise figure but the noise figure of all following stage should be divided by the total gain of previous stages. The linearity of low noise amplifier is also crucial because system linearity follows a similar relation as noise figure. Subsequent signal was demodulated by LO down to baseband and filtered then converted to digital signal via analog-to-digital converter (ADC) for further decode and processing in baseband processor.

4.2 Design and simulation of circulator

The circulator is built on one-side polished 4-inch silicon wafer. For the convenience of further integration of our design with existing CMOS technology, initially we chose material and thickness specification of ground, dielectric and transmission line following those of top three layers of IBM 180nm CMOS technology.

The circulator is a Y-junction shape device with ferrite thin film sandwiched in aforementioned two metal layers inside dielectric. We can remove the external biasing magnet giving credit to the strong internal field within ferrite material. In this design, the ferrite disk plays the double-role of high dielectric index anisotropic material and biasing magnet.

Considering the difficulty of fabrication, we did not use stripline or co-planar waveguide as transmission line because stripline requires buried metal in dielectric and co-planar waveguide requires very large area of ground connection. We chose microstrip line that is most easy to fabricate on wafer. The model of circulator is shown in Figure 4.2 and a cut is illustrated to show the layer cross view.

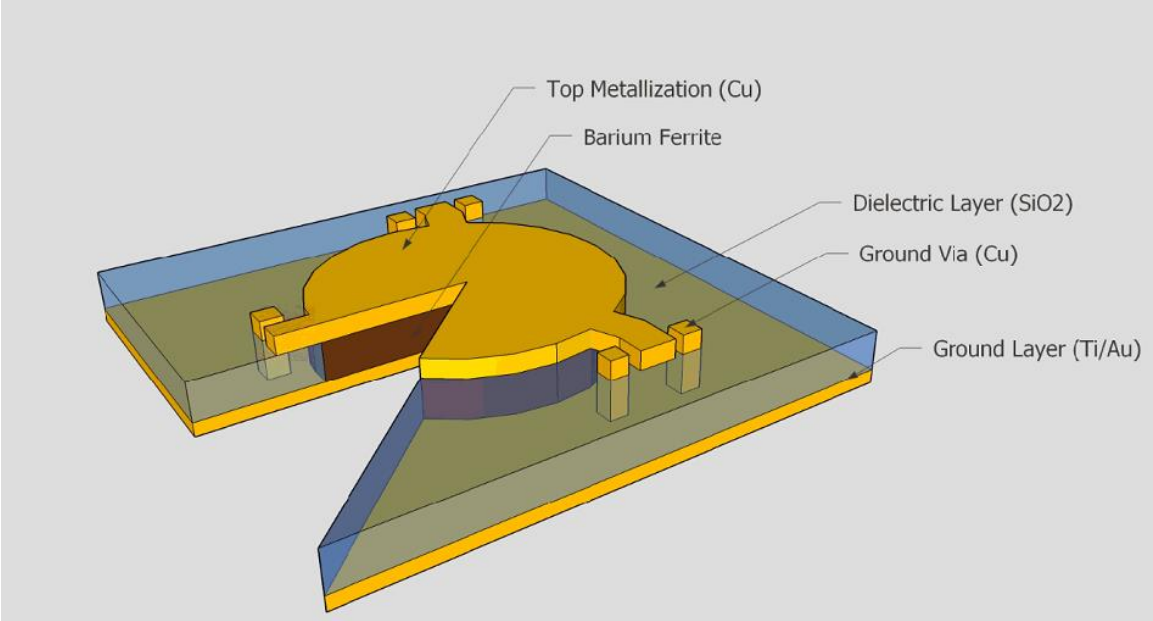

Figure 4.2 Three dimensional model of circulator design

A metal disk with radius R is placed on the layer and formed a resonator operating at desired frequency together with ferrite disk and ground layer underneath. By solving Maxwell equations involving the Bessel function of the Nth order, the dimensions of circulator can be calculated including the width of microstrip line and the radius of the ferrite disk. [37] The equations are as follows.

$$\sin\psi = \frac{W}{2R} = \frac{\pi Z_d}{1.84\sqrt{3}Z_{ferrite}}(-\kappa/\mu)$$

where ψ is the angle of edge where the microstrip line interacts with the center conductor as is shown in Figure 4.3. The width of microstrip line is denoted as W and the radius of the ferrite disk is denoted as R and it can be calculated as follows:

$$R = \frac{1.84\lambda}{2\pi\sqrt{\mu_{eff}\epsilon'}}$$

where μ_{eff} is the effective permeability in the magnetized ferrite and ϵ' is the real permittivity of the ferrite disk. Ideally three transmission lines form 120° with each other but two bands were added for the convenience of probing and measurement.

As calculated in Matlab program, the final dimension of circulator is shown in Table II

TABLE II: DIMENSION OF CIRCULATOR DEVICE

DIMENSION	**VALUE**	**UNIT**
Disk radius R	0.68	mm
Microstrip line width W	0.122	mm
Characteristic Impedance Z	50	ohm
Thickness of dielectric	5	μm
Thickness of ground	0.5	μm
Thickness of top metal	0.5	μm

Once the dimensions of the circulator have been set, it was modeled in CST and simulated with frequency domain simulator. The setting of parameters of material are listed in Table III.

TABLE III: PARAMETERS FOR CIRCULATOR SIMULATION

PARAMETERS	**SIZE**	**UNIT**
Dielectric constant of SiO2	3.9	
Dissipation factor of SiO2	0.001	
Dielectric constant of composite	4.41	
Dissipation factor of composite	0.005	
Frequency range	40-67	GHz
Dispersion model	Gyrotropic	
Mu infinity	1	H/m
Lande factor	2	
Saturation magnetization (4πM)	700	Gauss
Magnetic field vector (x, y, z)	(0, 0, 17500)	Oe

The simulation model and simulation results are shown in Figure 4.3, Figure 4.4 and Figure 4.5.

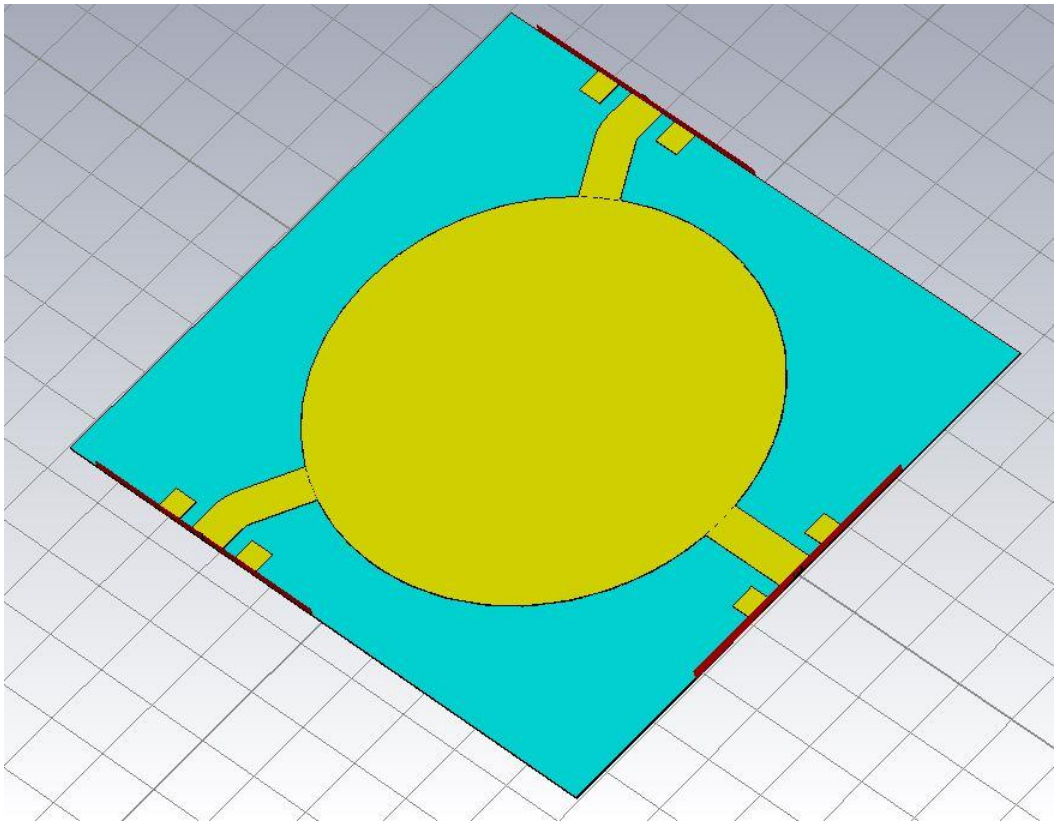

Figure 4.3 Circulator model in real aspect ratio in CST microwave studio

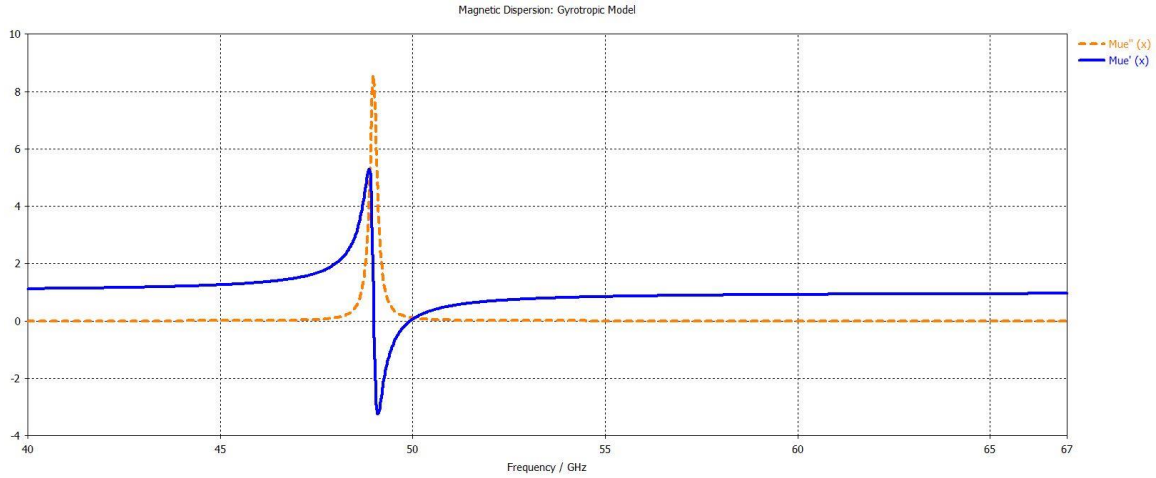

Figure 4.4 Gyrotropic model of ferrite permeability as simulated in CST microwave studio

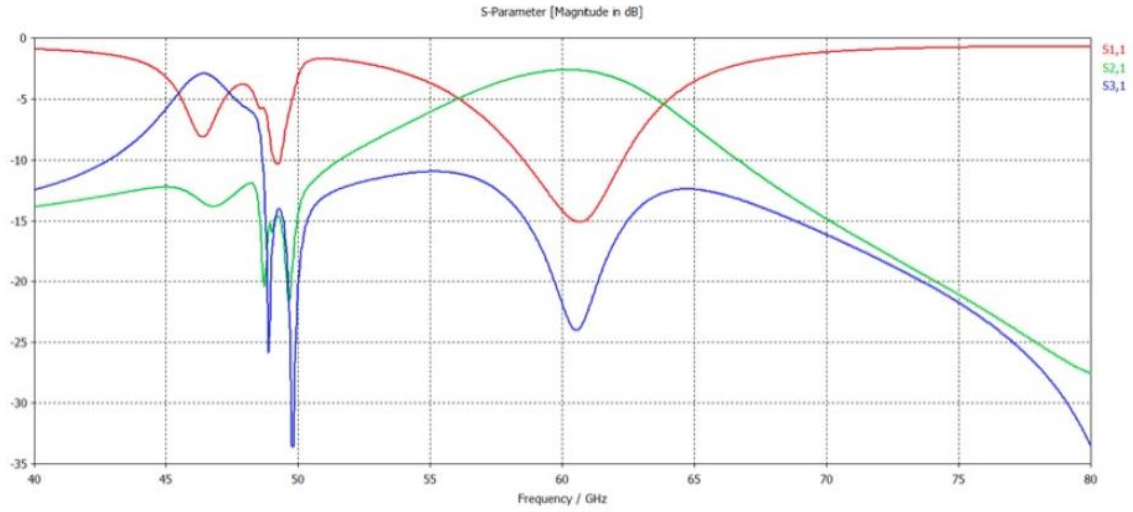

Figure 4.5 S-parameter results of 3-port circulator from 45GHz to 80GHz

From Figure 4.5 above, return loss at port 1 is -15dB at 61GHz. The insertion loss from port 1 to port 2 is 2dB and the isolation to port 3 is 23dB. It is easy to tell that power can be transferred from port 1 to port 2 with negligible loss and port 3 is isolated with over 20 dB attenuation. Since three ports are geometrically identical to each other, this non-reciprocal performance holds for all three ports thus the circulator can flow in a circulating manner.

4.3 Fabrication Detail of Circulator

The approach of fabrication the author took is building circulator “bottom-up” and starts from a bare Silicon wafer. Because of the difficulties of ferrite material patterning, two recipes of fabrication were developed and used. In this section, both recipes will be presented and discussed in detail. Circulator fabricated following one of the recipes was measured. Results and analysis will be presented in the next section.

4.3.1 Recipe one with lift-off patterning

As we discussed in the background chapter, the mostly efficient and preferred way to pattern a film is to transfer patterns by photoresist then implement etching as the photoresist layer acts as a mask.

However this standard process is not applicable in this situation of circulator fabrication: composite material is made from ferrite nanopowder and AZ9260 photoresist as polymer, if we keep using the aforementioned photolithography, composite material will be stripped away together with mask photoresist either by soaking in organic solvent or burnout in resist asher.

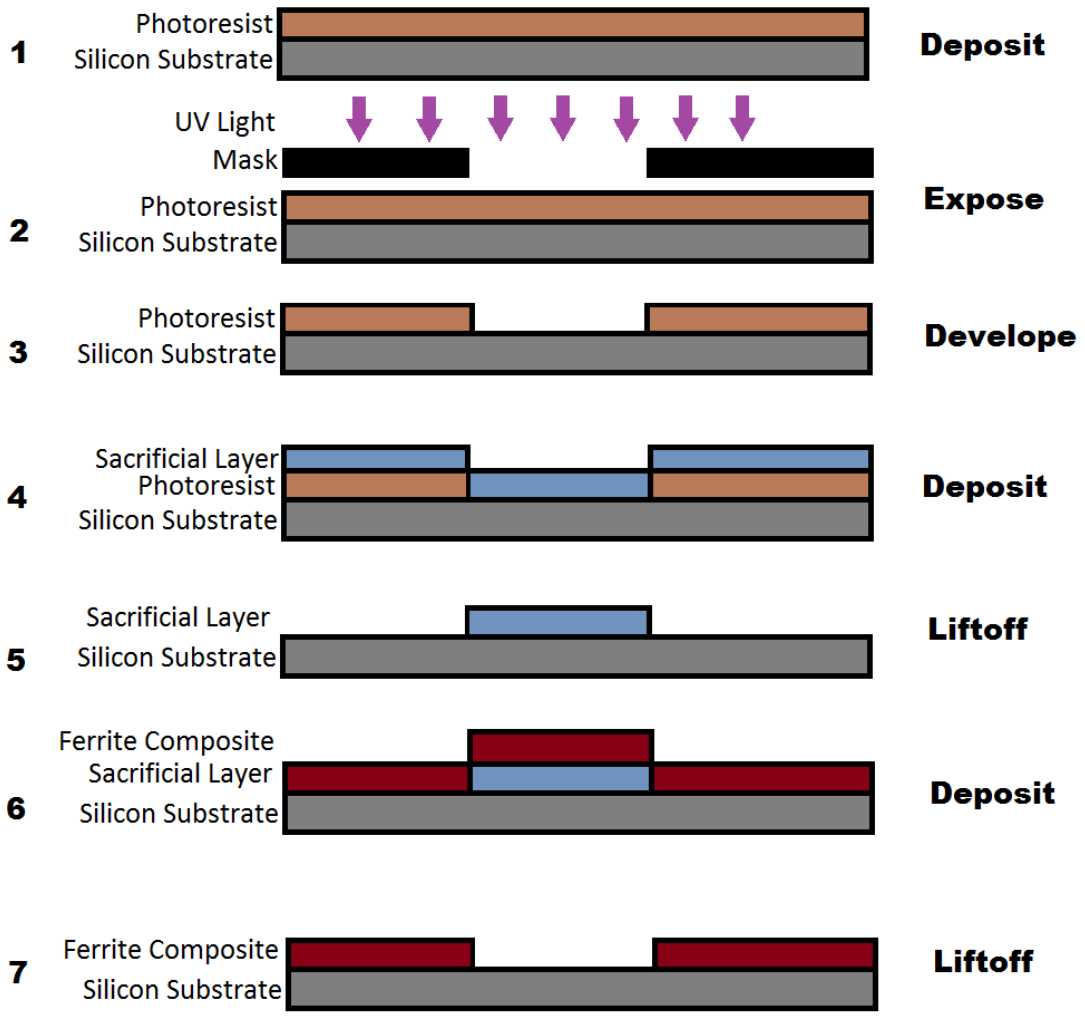

Figure 4.6 Process flow of double liftoff patterning

There is another patterning process that is not involved in direct etching of composite or direct contact of photoresist with composite [38]. This process employed two sacrificial materials to lift-off unwanted ferrite material, which can be better illustrated in Figure 4.6.

TABLE IV
RECIPE ONE WITH LIFTOFF PATTERNING

Step	Description	Notes
Cleaning	Ultrasonic cleaner	@Tufts
Metallization	Deposit 20 nm Titanium and 480nm gold	EE-4 @Harvard or sputter tools @Tufts
Dielectric layer	Deposit 4um SiO2	CVD-3 @Harvard

Photolithography-1	Spin cast resist, prebake, expose mask 1 (transparent at via) develop and post-bake	@Tufts Thick AZ series PR
Etch Oxide	Silicon dioxide etching	RIE-8 @Harvard
Strip	Strip photoresist	@Tufts
Electroplate	Carefully control thickness by periodically measure it under interferometer	@Tufts
Clean	O2 cleaning after stripping	RIE @Tufts
Photolithography-2	Spin cast resist, prebake, expose mask 2 (transparent at center disk), develop, post-bake	@Tufts Thick AZ series photoresist
Clean	O2 cleaning after develop	RIE@Tufts
Etch Oxide	Silicon dioxide etching	RIE-8 @Harvard
Strip	Strip photoresist	@Tufts
Photolithography-3	Spin cast resist, prebake, expose mask 3 (opaque at central pad), develop, post-bake	@Tufts Thin SPR series photoresist
Metal	Deposit 1000nm aluminum	TE @Harvard
Liftoff	Liftoff resist (and aluminum upon it)	@Tufts
Spin-coating	Spin ferrite and photoresist, add bias magnets and bake	@Tufts
Liftoff	Liftoff aluminum (and ferrite upon it)	@Tufts
Metal	Deposit 20nm titanium and 480nm gold using shadow mask (signal pad and transmission line)	EE4@Harvard

Step one of double liftoff is to deposit and pattern a layer of photoresist in the area that needs to be covered by ferrite composite at last. Then a thin layer of metal sacrificial layer was deposited on top of existing photoresist. The next step is to soak and rinse in organic solvent such as acetone so that photoresist was dissolved and metal lay down upon photoresist was “liftoff” together with it. However metal that has no photoresist layer underneath will survive this process and a negative pattern of metal was obtained. Then a layer of ferrite composite was deposited and afterward the whole wafer was etched in specific etchant so that metal was removed and lifted off unwanted photoresist above it.

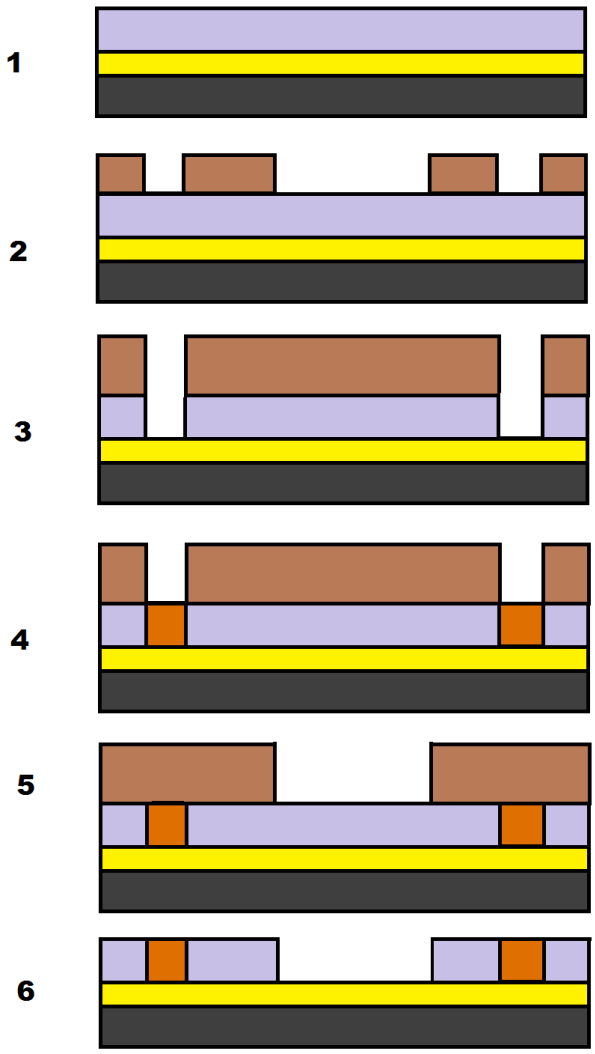

Figure 4.7 Process of ground metallization and dielectric deposition (#1), first lithography (#2), dielectric etching (#3), via plate filling (#4), Second lithography (#5) and center disk etching (#6)

Based on double liftoff process, a complete recipe of circulator fabrication was developed as shown in Table IV.

Before doing any process on the silicon wafer, a thorough wafer cleaning is preferred. In this work, wafer was cleaned in acetone, isopropanol and deionized water in beaker placed in ultrasonic cleaner sequentially. Bare wafer was blew dry and deposited metallization and dielectric took place at Harvard University.

Metal layers of Titanium (20nm) followed by gold (480nm) were deposited employing an e-beam evaporator. The function of titanium is to ease the poor adhesion issue of gold with bare silicon wafer. Amorphous silicon dioxide layer with 4000nm thickness was deposited employing a Chemical Vapor Deposition. The dielectric constant of grown silicon diode is 3.9. Flatness of as-deposit material was checked by laser ellipsometer and the variation of thickness was below 10nm.

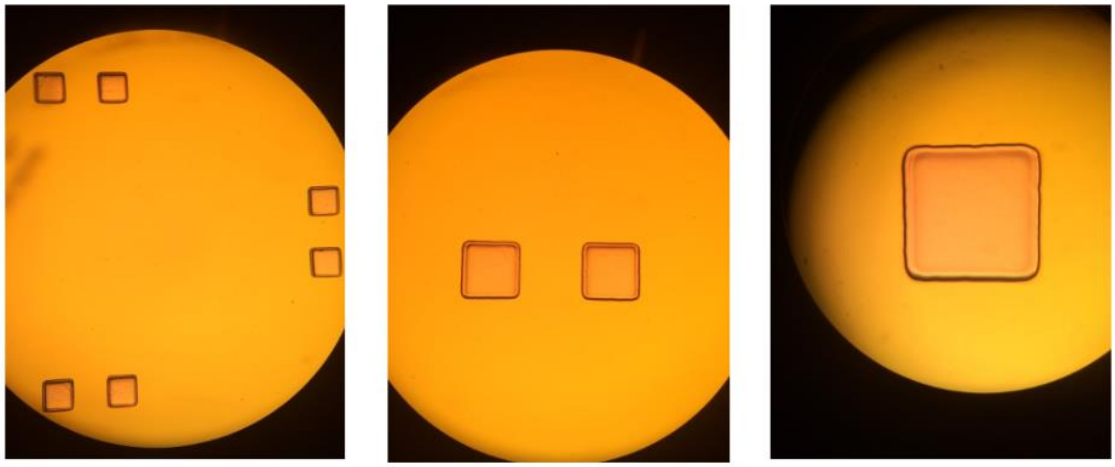

Figure 4.8 Microscopic photos of fabricated ground vias for probe landing

In the first lithography, area of ground vias were exposed and etched employing reactive iron etcher. The recipe of precursor gases are as follows:

C_4F_8: 10 standard cubic centimeters per minute (sccm)

SF_6: 10 sccm

H_2: 3 sccm

After etching through the dielectric and reach the ground layer, wafers were plated in copper plating solution made from copper sulfate and sulfuric acid. The plating current was controlled to be small (~5uA) so did the plating deposition rate, which is critical to achieve good quality.

Wafers processed at step 4 are shown in microscopic photo in Figure 4.8

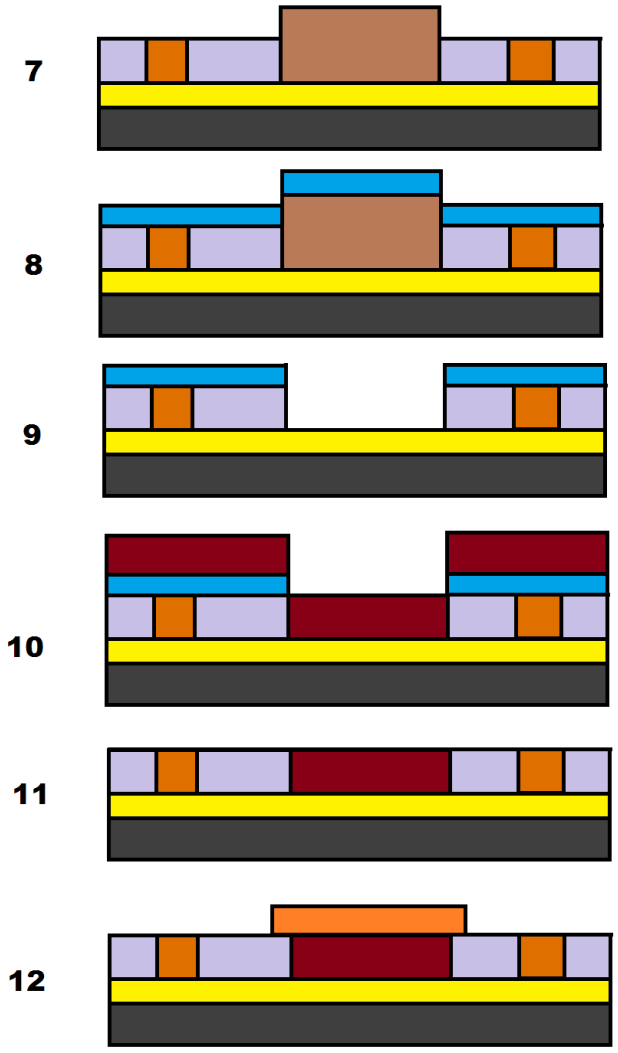

Figure 4.9 Process of 3rd lithography (#7), aluminum sacrificial layer deposition (#8), 1st liftoff (#9), ferrite composite deposition (#10), 2nd liftoff (#11) and transmission line deposition (#12)

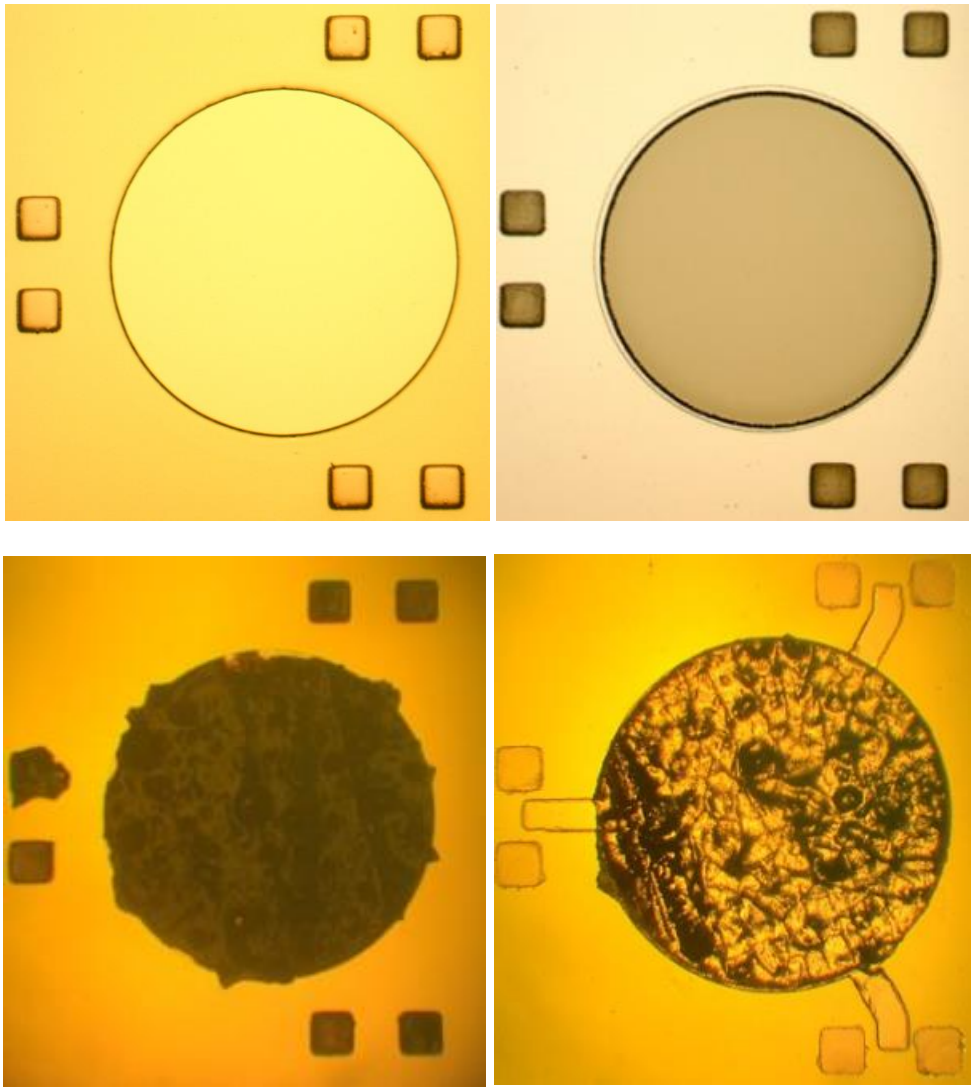

Figure 4.10 Microscopic photo of circulator after center disk was etched (top left), after aluminum deposition (top right), after double-liftoff was finished (bottom left) and after transmission line metallization (bottom right)

In the third lithography, etched center disks are protected with photoresist. Then a layer of thick (1um) aluminum was deposited employing thermal evaporation. Right after evaporation, photoresist was liftoff using acetone and formed a negative pattern of aluminum sacrificial layer. Double liftoff was implemented by first spin-casting photoresist composite prepared as introduced in section 3.2. Note that during hot baking of ferrite composite on wafer, a 4'' neodymium magnet with residue induction $Br_{max} = 13400$ Gauss was used during baking to provide biasing field with

direction perpendicular to substrate plane. The next step was to liftoff sacrificial layer with mild Aluminum Etchant Type D ordered from Transene that is compatible with Titanium, gold and copper.

The microscopic photos of the circulator after some critical processes are shown in Figure 4.10. Note that after double-liftoff, because of a) the low homogeneity of ferrite composite, b) the thickness of spin-cast film is much thicker than expected and c) the low liftoff speed of sacrificial layer, we faced the issue of unsuccessful patterning. The contour of the circulator was not smooth and pores and holes of ferrite caused a DC short from transmission line to ground.

The three masks used in recipe one are shown in Figure 4.11. Note that dark and white shaded areas are transparent and red colored areas are opaque to UV light.

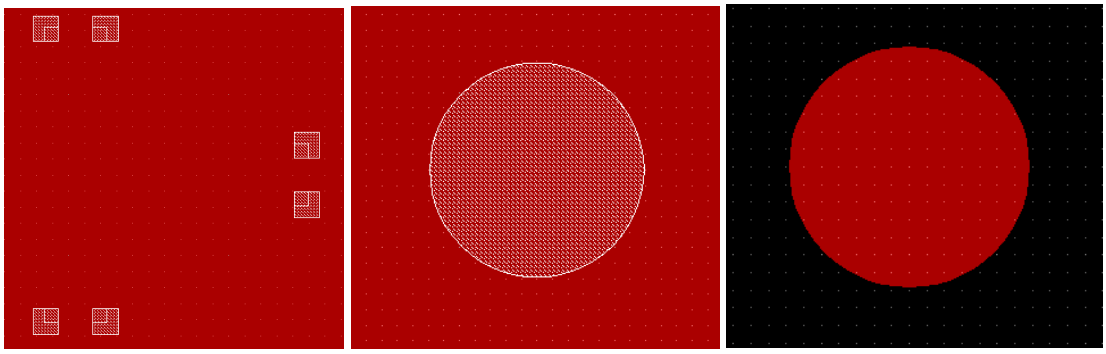

Figure 4.11 Mylar mask design for first (left), second (middle) and third (right) lithography

4.3.2 Recipe Two with Chemical-Mechanical Planarization (CMP)

For the purpose of alleviating the difficulty of ferrite patterning, we developed another recipe that employed Chemical-Mechanical Planarization to assist ferrite patterning. The complete recipe of CMP assisted patterning is shown in Table V.

Note that recipe two can take full advantage of photolithography masks #1 and #2 from recipe one, and CMP process saved a large amount of time and energy, which is explicit from the length of recipe.

TABLE V
RECIPE TWO WITH CHEMICAL MECHANICAL PLANARIZATION

Step	Description	Notes
Cleaning	Ultrasonic cleaner	@Tufts
Metallization	Deposit 20 nm Titanium and 480nm gold	EE-4 @Harvard or sputter tools @Tufts
Dielectric layer	Deposit 4um SiO2	CVD-3 @Harvard
Photolithography-1	Spin cast resist, prebake, expose mask 1 (transparent at via and central pad), develop, post-bake	@Tufts Thick AZ series PR
Etch Oxide	Silicon dioxide etching	RIE-8 @Harvard
Electroplate	Carefully control thickness by periodically measure it under interferometer	@Tufts
Strip	Strip photoresist	@Tufts
Clean	O2 cleaning after stripping	RIE @Tufts
Photolithography-2	Spin cast resist, prebake, expose mask 2 (transparent at via), develop, post-bake	@Tufts Thick AZ series photoresist
Clean	O2 cleaning after develop	RIE@Tufts
Strip	Strip photoresist	@Tufts
Spin-coating	Spin ferrite and photoresist, add magnets and bake	@Tufts
CMP	Polishing deposited ferrite layer down to dielectric surface	@Entrepix
Metal	Deposit 20nm titanium and 480nm gold using shadow mask (signal pad and transmission line)	EE4@Harvard

Chemical-Mechanical Planarization is a hybrid method of chemical etching and physical polishing. During polishing of wafer on special-made pad, prepared abrasive and corrosive slurry is fed to interface in order to remove unwanted material uniformly [39].

The first half of this recipe is exactly the same as recipe one until the finish of ground vias fillings. The second half of double-liftoff was replaced by simple CMP process as depicted in Figure 4.12.

The spin-casting of ferrite composite was same as presented in recipe one. The chemical polishing was outsourced to Entrepix, AZ. After Entrepix processed and shipped wafers back, final metallization of transmission line was done same as Recipe one.

The Circulator processed after CMP is shown in Figure 4.13 and the fabricated circulator after transmission line metallization is shown in Figure 4.14.

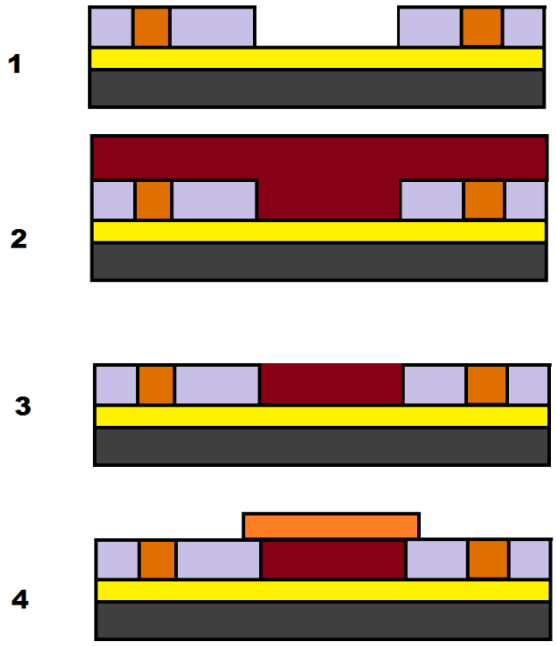

Figure 4.12 Process of Electroplated ground via fillings (#1), ferrite composite spin-casting (#2), Chemical-Mechanical Planarization (#3) and transmission line metallization (#4)

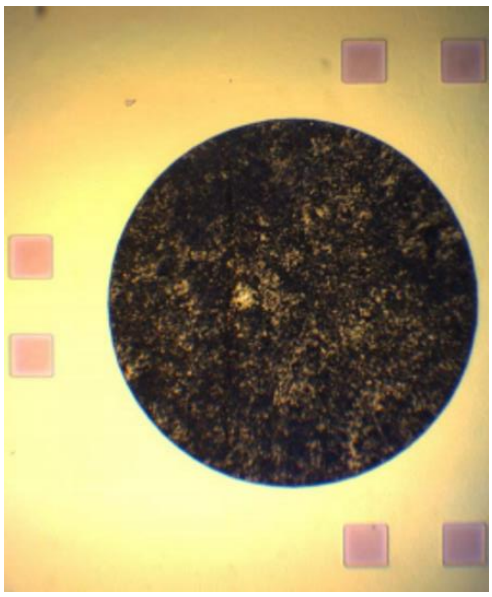

Figure 4.13 Microscopic photo of device after Chemical-Mechanical Planarization

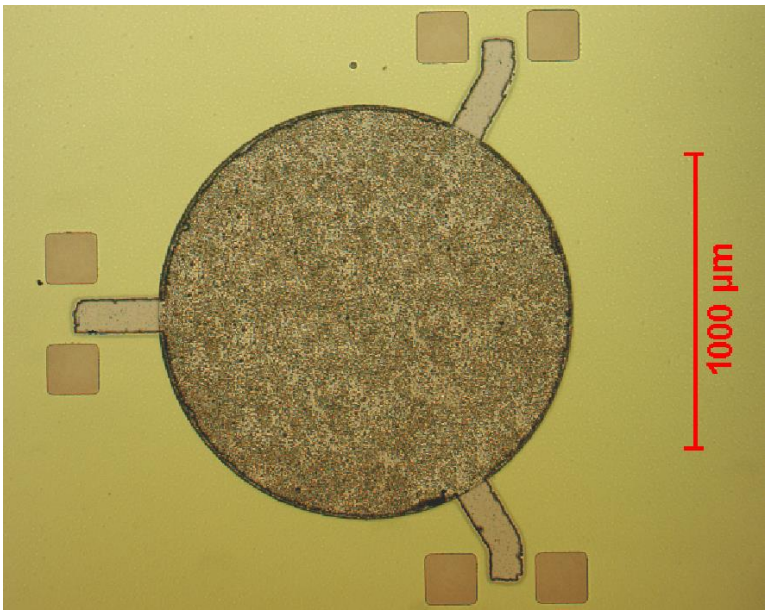

Figure 4.14 Microscopic photo of fabricated circulator on wafer

By running Chemical-Mechanical Polishing, the surfaces of ferrite composite were flatter than double recipe, because during polishing composite film was planarized under pressure. The contour

of ferrite disk was also complete and smooth. We didn't get the DC shorting issue in this case. The measurement settings and analysis of results will be discussed in Chapter 5

Chapter 5 Results and Analysis

5.1 Measurement setting

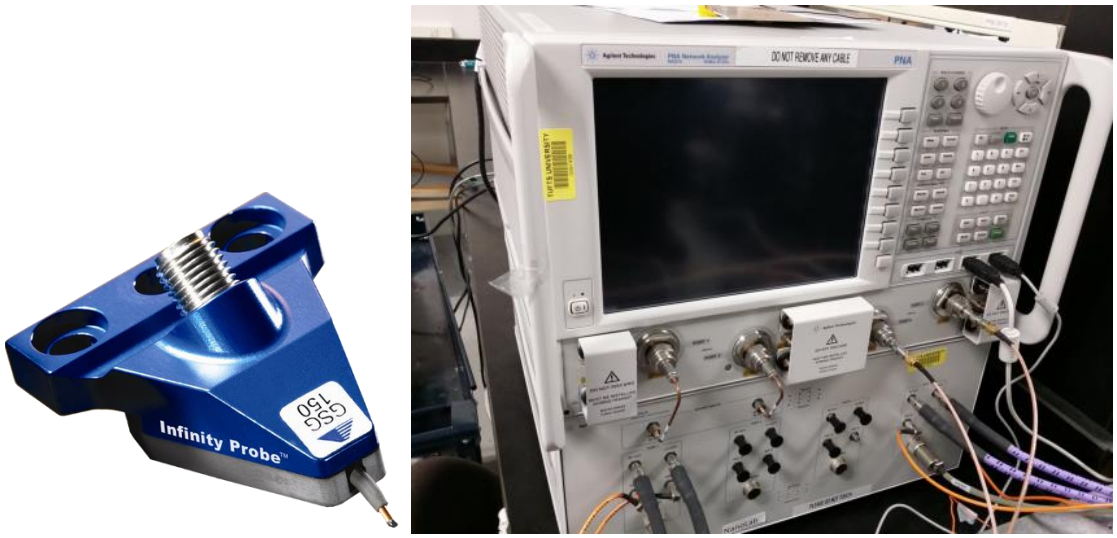

Figure 5.1 Probe from CascadeMicrotech and N5227A network analyzer from Keysight

To test the fabricated circulator, a 4-port Keysight network analyzer N5227A which was capable of measuring from 10MHz to 67GHz was employed to measure the 3-port S-parameter. Three Infinity probes were ordered from CascadeMicrotech that cover 67GHz as well. The pattern of probe tip is Ground-Signal-Ground (GSG) with 150um pitch size, which is suitable to this design. Three ultra-low loss cables from Megaphase were ordered to accommodate testing needs. In order to safely land probe onto landing pad, a three arms CascadeMicrotech probe station was employed to handle the probe. It features a mini vacuum pump capable of limiting the movement wafer during probing. And a colored microscopic monitor to assist probe landing. Photos of Infinity probe and network analyzer employed are shown in Figure 5.1

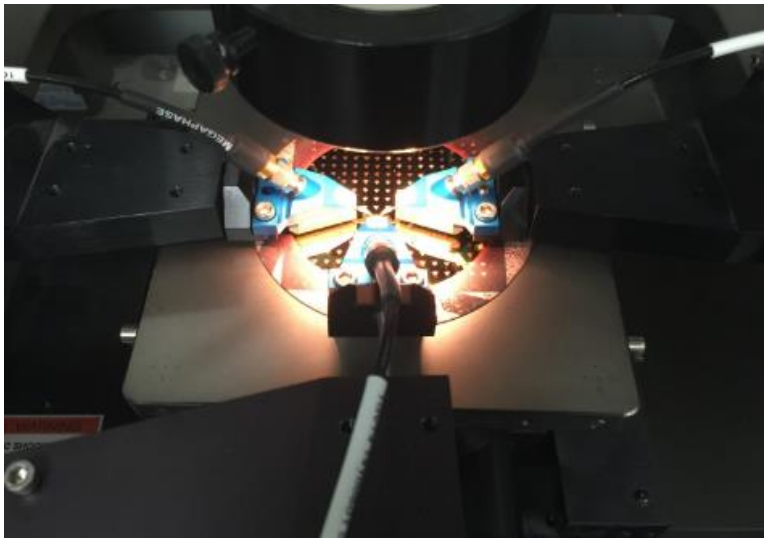

Figure 5.2 Photo of circulator on-wafer probing setting during measurement

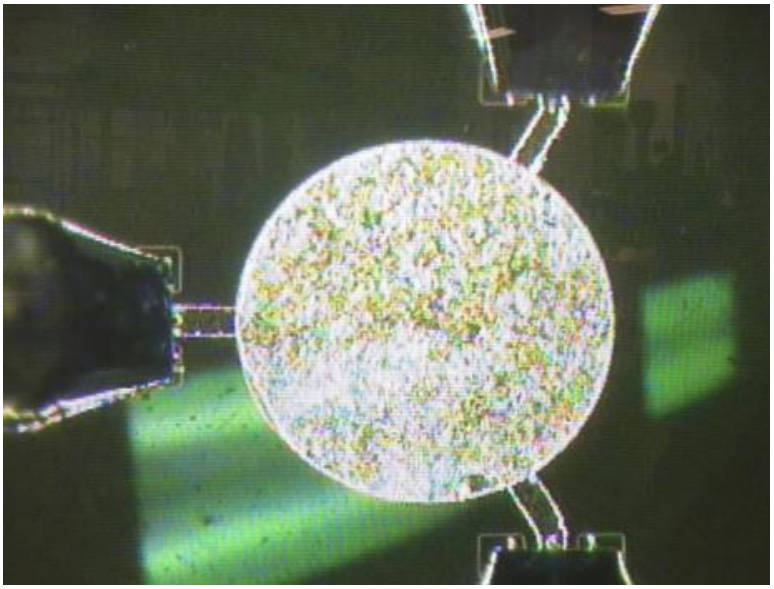

Figure 5.3 Microscopic view of fabricated circulator under test

The photos of probing and microscopic view of probed circulator are shown in Figure 5.2 and Figure 5.3 respectively.

Three out of four ports of network analyzer were used to determine the 3-port S-parameter of circulator from 10-67GHz. Before measurement, three probes were calibrated in pairs three times

so that the insertion loss and phase offset of cables and probes were de-embedded. The measurement results are shown in next section.

5.2 Results of Circulator on Wafer

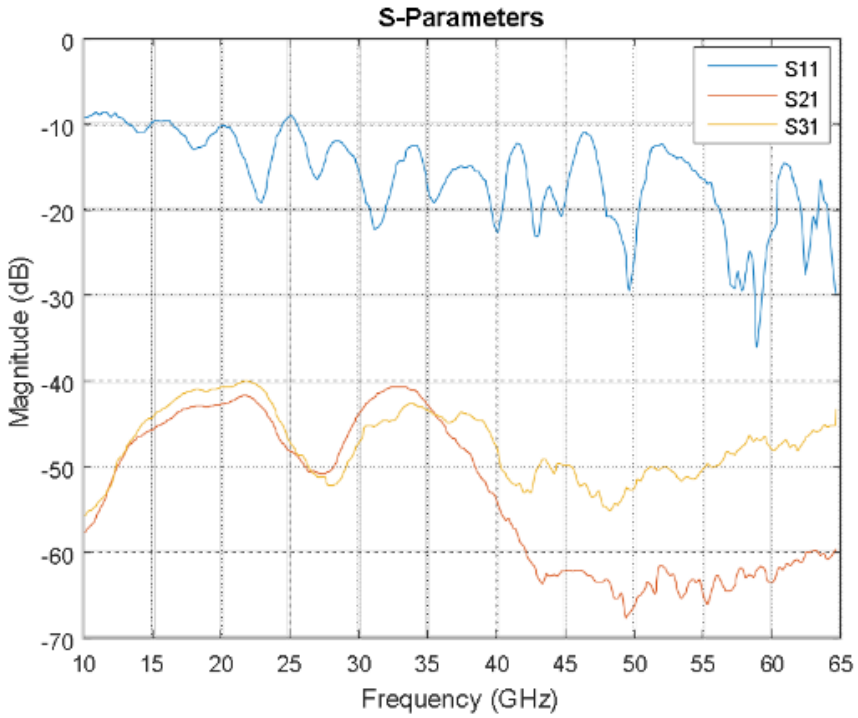

Figure 5.4 Measured S-parameter of circulator

The measured S-parameter of fabricated circulator can be found in Figure 5.4. According to measurement results, the isolation of two path (S21 and S31) is around 15dB, which correlated with simulation. However the overall Insertion loss is way higher than the expected 2dB, so does the return loss at port.

The root causes of deviation from simulation are studied and listed as follows:

a) The loss mechanism of ferrite composite was underestimated

Comparing to their crystallized counterpart, ferrite composite shows less homogeneity and flatness at micro- and nano scale. The SEM image of spin-casted composite surface shown in Figure 5.5 is a proof. At 60GHz, any grain or hole is a source of loss. Meanwhile, the magnetic loss caused by the wide linewidth of ferromagnetic resonance was also underestimated and poorly modeled in full EM solver. The reported linewidth of screen-printed thick film Barium hexagonal ferrite film is 320 scale and it was already believed lossy to microwave frequency range applications [40]. Ferrite composite deposited by spin-casting shows linewidth several times wider than screen-printing. This is another root cause of loss.

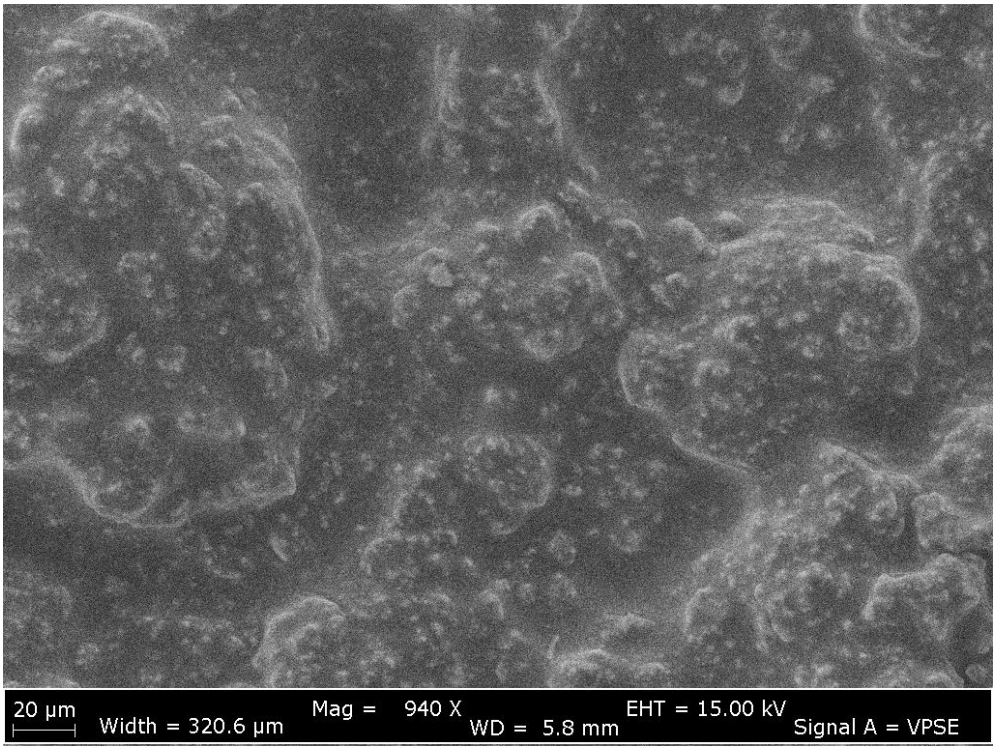

Figure 5.5 Scanning Microscopy Image of ferrite composite surface

b) The Chemical-Mechanical Planarization process over-polished ferrite material

Although the loss of ferrite film was underestimated, another contributor to unexpected loss is the over-polished surface after CMP. Partly because of the low density and low adhesion to

surface, center ferrite disks were polished away by 1um, which is 25% of all ferrite material as designed.

c) The thickness of evaporated metal is too thin for probe landing

Limited by evaporator capability, the thickness of evaporated metal as transmission line was only 3um, which is much lower than plated metal. The deposited microstrip lines were more dispersive and lossy, which contributed to overall loss.

d) Characteristic impedance of microstrip line mismatched with probe

The characteristic impedance of designed microstrip line was only 2.5ohm, which is limited by the minimum width that can be deposited by using shadow mask. In order to increase the characteristic impedance to 50 ohm as probe, new type of transmission line such as co-planar waveguide has to be developed to replace the microstrip line.

Chapter 6 Conclusion

6.1 Future Work

The work outlined in this thesis was sponsored by the National Science Foundation under grant ECCS-1390894. This project will run for an additional one year. During the next year, to alleviate the loss problem of fabricated circulator, a possible solution is to experiment with a new ferrite deposition method. In Chapter 2 and Chapter 3, various types of deposition process were reviewed.

However for whatever existing process, there lies a paradox that we could not achieve all appealing properties of this material in a single type of film. Generally in single crystal film, magnetic domains are better aligned showing stronger anisotropic field, and resonant linewidth can be as narrow as tens of Oersted, while on the other hand, properties like self-bias and strong remnant magnetization are inherent in polycrystalline material [17]. Since we are targeting at future integration of a non-reciprocal device with existing IC technology, weightless self-biased property is of our highest concern. On the other hand, techniques such as screen printing and spin-casting that employ Micro or Nano powder have out-of-plane self-bias properties with high RR in the range of 0.7-0.95 but the down part of such techniques is the wide resonance linewidth (i.e. loss in material), usually in 300-500 Oe range. Another drawback of such techniques is high porosity and surface roughness, which is a killing source of loss in a practical microwave device.

We conclude that all aforementioned existing techniques fall into one of the three categories of shortcoming.

a) Such techniques can grow very good quality single crystal film with reasonable thickness but cannot achieve self-biasing or can only achieve in-plane self-biasing (Liquid Phased Epitaxy, Pulsed Laser Deposition)
b) Such techniques can grow good quality film but have very poor growth rate or requires uncommon substrate that is unable to integrate with. (Sputtering, Pulsed Laser Deposition, ATLAD)
c) Such techniques can only deposit moderate or poor quality films whose porosity and roughness condition highly deteriorate device performance. (Screen printing, spin casting)

Besides what have been already discussed, there is another thin film preparation technique named spray pyrolysis that needs our attention. Spray pyrolysis is a process in which a thin film is deposited by spraying a solution on a heated surface, where the constituent reacts to form a chemical compound [41-43]. A highly adherent and homogeneous poly-crystalline Barium ferrite thin film is formed at deposition rate 40-100 nm/mins.

As reported by Sankaranarayanan et al [42], the as deposited film on quartz plate which was heated to 350-400°C has superparamagnetic behavior. During post annealing, the ferrite crystalline starts to nucleate and a narrow hysteresis loop is observed after annealing at 650°C for 3 h. As annealing temperature and duration increase, the hysteresis loop expands and such films show good coercivity and remanence ratio.

Film deposited by employing spray pyrolysis and annealing is poly-crystalline featuring both narrow linewidth and large remanence ratio, the out-of-plane full demagnetization effect in single crystal film can be avoided in such films.

6.2 Summary

This thesis presents the work that has been done in designing, simulating, fabricating and testing of a self-bias, on-chip barium ferrite circulator operating at 60GHz unlicensed band toward next generation wireless communication. By taking advantage of the strong non-reciprocal field within Barium hexagonal ferrite, a self-bias feature was realized on this device and consequently less weight, size and cost was achieved. This device features 2mm by 2mm miniaturization size, which is the smallest ever reported at this frequency range.

The fabricated device was tested by on-wafer probing and 15dB non-reciprocal isolation was measured. These positive results are an encouraging sign toward full integration of a circulator with existing IC technology and this circulator may play an important role in wireless communication as port of a front-end module.

Bibliography

[1] A. Saib, M. Darques, L. Piraux, D. Vanhoenacker-Janvier, and I. Huyner. An unbiased integrated microstrip circulator based on magnetic nanowired substrate. Microwave Theory and Techniques. IEEE Transactions on, 53(6):2043-2049, June 2005

[2] Farview Microwave, SMA circulator with 17dB isolation from 1 GHz to 2 GHz and 10 Watts, Product datasheet, Farview Microwave.

[3] Federal Communication Comission, Rules for unlicensed operation in the 57-64 GHz Band, FCC Record: FCC-13-112A1_Rcd

[4] Afif Osseiran, Scenarios for 5G mobile and wireless communications: the vision of the METIS project, Communication Magazin, IEEE. 52 (5). Doe:10.1109/MCOM.2014.6815890

[5] Bin Peng, Wenxu Zhang, Yanlong Sun, Jingjie Lin, Wanli Zhang, and Hui Li. Design of microstrip Y-junction circulator based on ferrite thin films. In Microwave Conference Proceeding (CJW), 2011 China-Japan Joint, pages 1-4, April 2011

[6] David M Pozar. Microwave engineering. John Wiley & Sons, 2009

[7] Philips Semiconductor. Circulator and isolator, unique passive devices. Application Note AN98035, 1998

[8] Douglas K. Linkhart. Microwave circulator design. Artech House, Norwood, A, 1989. ID:19456097

[9] Gerald F. Dionne, Gary A, Allen, Pamela R. Haddad, Caroline A. Ross and Benjamin Lax, Circular Polarization and Nonreciprocal Propagation in Magnetic Media, Lincoln Laboratory Journal, Volume 15, Number 2, 2005

[10] Ümit Özgür, Yahya Alivov, Hadis Morkoç, Microwave ferrites, part 1: fundamental properties, Journal of Material Science: Material in Electronics (2009) 20:789-834

[1] R. C. Legraw, E. G. Spencer and C. S. Porter, Ferromagnetic resonance linewidth in Yttriu iron garnet single crystals, Physical Review, Vol 110 Iss.6, June 1958

[12] J Goulon; A Rogalev; F Wilhelm; G Goujon; A yaresko; Ch Brouder & J Ben Youssef, Site-selective couplings in x-rag-detected magnetic resonance spectra of rare-earth-substituted yttrium iron garnets, New Journal of Physics. pp.1-30 April 2015

[13]C. G. Willson, R. R. Dammel and A. Reiser, Photoresist materials: a historical perspective, Advances in Resist Technology and Processing XIV: 28 (July 7, 1997) doe:10.117/12.275826

[14]R. Behrisch, Sputtering by particle bombardment, Springer, Berlin. ISBN 978-3-540-10521-3

[15] Jason Tavares, E. J. Swanson, S. Coulombe, Plasma Synthesis of Coated Metal nanoparticles with Surface Properties Tailored for Dispersion, Plasma Processes and Polymer. 5 (8): 759. Doe:10.1002/ppap.20080074

[16] A. Y. Cho, Growth of III/V semiconductors by molecular beam epitaxy and their properties, Thin Solid Films, vol. 100, pp. 291-317, 1983

[17] Vincent G. Harris, Anton Geiler, Yajie Chen, Soack Dae Yoon, Mingzhong Wu, Aria Yang, Zhaohui Chen, Peng He, Patanjali V. Parimi, Xu Zuo, Car E. Patton, Manasori Abe, Olivier Acher,

Carmine Vittoria, Recent advances in processing and applications of microwave ferrites, Journal of Magnetism and Magnetic Material, 321 (2009) 2035-2047

[18] L. Zhang, X. D. Su, Y. Chen, Q. F. Li, V. G. Harris, Radio-frequency magnetron sputter-deposited barium hexaferrite fil on Pt-coated Si substrates suitable for microwave application, Journal of Magnetism and Mganetic Materials, Volumn 211, Issues 1-3, March 2000.

[19] I Wane, A Bessaudou, F Cosset, A Célérier, C Girault, J.L Decossas, J.C Vareille, "Thick barium hexaferrite (Ba-M) films prepared by electron-beam evaporation for microwave application", in *Journal of Magnetism and Magnetic Materials*, Volume 211, Issues 1–3, 1 March 2000

[20] Song, Young-Yeal and Kalarickal, Sangita and Patton, Carl E., "Optimized pulsed laser deposited barium ferrite thin films with narrow ferromagnetic resonance linewidths",in *Journal of Applied Physics*, 94, 5103-5110 (2003)

[21] A. L. Geiler, S. D. Yoon, Y. Chen, A. Yang, C. N. Chinnasamy, M. Geiler, V. G. Harris and C. Vittoria, Alternating target laser ablation deposition of high quality barium hexaferrite thin films from barium monoferrite and hematite targets, *Journal of Applied Physics*, 103, 07B914 (2008)

[22] Song, Young-Yeal and Das, Jaydip and Wang, Zihui and Tong, Wei and Patton, Carl E.,"In-plane c-axis oriented barium ferrite films with self-bias and low microwave loss", in *Applied Physics Letters*, 93, 172503 (2008)

[23] Yoon, S. D. and Vittoria, C."Thick M-type barium hexaferrite films grown on garnet substrates", in *Journal of Applied Physics*, 96, 2131-2135 (2004)

[24] Chen, Yajie and Geiler, Anton L. and Chen, Taiyang and Sakai, Tomokazu and Vittoria, C. and Harris, V. G., "Low-loss barium ferrite quasi-single-crystals for microwave application", in *Journal of Applied Physics*, 101, 09M501 (2007)

[25] Liu Chao; Sholiyi, O.; Afsar, M.N.; Williams, J.D., "Characterization of Micro-Structured Ferrite Materials: Coarse and Fine Barium, and Photoresist Composites," in *Magnetics, IEEE Transactions on* , vol.49, no.7, pp.4319-4322, July 2013

[26] International Communication Union Recommendations, Recommendation P.676, Approved in Sep. 2013.

[27] PFM Smulders. Exploiting the 60 GHz for local wireless multimedia access: prospects and future directions, Communications Magzine, IEEE, 40(1): 140-147, 2002

[28] A.A. Volkov, Y.G. Goncharov, G.V. Kozlov, S.P. Lebedeve, and A.M. Prokhorov. "Dielectric measurement the submillimeter wave-length region." Infrared Physics, 1985: 369-373.

[29] K. N. Kocharyan, M. Afsar and I. I. Tkachov, Millimeter wave magnetioptic: New method for characterization of ferrites in the millimeter-wave range, IEEE Transaction of Microwave Theory and Tech. 1999: 2636-2643

[30] Liu Chao, Anjali Sharma and Mohammed N. Afsar, Microwave and Millimeter wave ferromagnetic absorption of nanoferrites, Transaction on Magnetics, 2012: 2773-2776.

[31] J. R. Birch, G. J. Simons, M. N. Afsar, All intercomparison of measurement techniques for the determination of the dielectric properties of solid at near millimeter wavelengths, Transation on Microwave Theory and technique, 1994

[32] E. Schlömann, Microwave behavior of partially magnetized ferrites, Journal of Applied Physics, 1970: 204-214

[33] Ümit Özgür, Yahya Alivov, Hadis Morkoç, Microwave ferrites, part 2: Passive component and electric tuning, Journal of Material Science: Material in Electronic (2009) 20:911-952. DOE 10.1007/s10854-009-9924-1

[34] D. Wolpert and P. Ampadu, Managing Temperature Effects in Nanoscale Adaptive Systems, Springer, 2012, XXII, 174 p., ISBN: 978-1-4614-0747-8

[35] A. Christou, Reliability of High Temperature Electronics, RIAC, 1996, P444, ISBN: 978-0-9652-6694-9

[36] Shu Chen, Mohammed N. Afsar and Darin Sakdatorn, Dielectric-parameter of measurements of SiC at millimeter and submillimeter wavelengths, Transaction on Instrumentation and Measurement, April 2008: 706-715

[37] H. Bosma, On stripline y-circulator at uhf, IEEE Transactions on Microwave Theory and Technique, 12(1):61-72, Jan 1964

[38] Stephen D. Senturia, Microsystem Design, Springer US, P689, ISBN: 1475774583

[39] S. Wolf, Silicon processing for the VLSI Era, Vol. IV: Deep-submicron Process Technology, pp. 313-432, Lattice Press, 2002, ISBN: 9778-0961672171

[40] Yajie Chen, Tomokaze Sakai, Taiyang Chen, Soack D. Yoon, Carmine Vittoria and Vincent G. Harris, Screen printed thick self-biased, low-loss, bariu hexaferrite films by hot press sintering

[41] T González-Carreño, M.P Morales, C.J Serna, "Barium ferrite nanoparticles prepared directly by aerosol pyrolysis", *Materials Letters*, Volume 43, Issue 3, April 2000

[42] V.K Sankaranarayanan, R.P Pant, A.C Rastogi, "Spray pyrolytic deposition of barium hexaferrite thin films for magnetic recording applications", *Journal of Magnetism and Magnetic Materials*, Volume 220, Issue 1, October 2000

[43] Min Ha Kim, Dae Soo Jung, Yun Chan Kang, Jeong Hoo Choi, "Nanosized barium ferrite powders prepared by spray pyrolysis from citric acid solution", *Ceramics International*, Volume 35, Issue 5, July 2009